

1 **Quantification of hydraulic trait control on plant hydrodynamics and risk of hydraulic**
2 **failure within a demographic structured vegetation model in a tropical forest (FATES-**
3 **HYDRO V1.0)**

4 Chonggang Xu¹, Bradley Christoffersen², Zachary Robbins¹, Ryan Knox³, Rosie A. Fisher⁴,
5 Rutuja Chitra-Tarak¹, Martijn Slot⁵, Kurt Solander¹, Lara Kueppers^{3,6}, Charles Koven³, Nate
6 McDowell^{7,8}

7 1: Earth and Environmental Sciences Division, Los Alamos National Laboratory, Los Alamos
8 NM, USA

9 2: School of Integrated Biological and Chemical Sciences, University of Texas Rio Grande
10 Valley, TX, USA

11 3: Lawrence Berkeley National Laboratory, Berkeley, CA USA

12 4: CICERO Centre for International Climate Research, Oslo, Norway

13 5: Smithsonian Tropical Research Institute, Apartado 0843-03092, Balboa, Ancon, Republic of
14 Panama

15 6: Energy and Resources Group, University of California, Berkeley, CA USA

16 7: Atmospheric Sciences and Global Change Division, Pacific Northwest National Laboratory,
17 Richland, WA, USA

18 8: School of Biological Sciences, Washington State University, Pullman, WA, USA

19

20

21

22

23 Corresponding author: Chonggang Xu (cxu@lanl.gov)

24

25 **Abstract:** Vegetation plays a key role in the global carbon cycle and thus is an important
26 component within Earth system models (ESMs) that project future climate. Many ESMs are
27 adopting methods to resolve plant size and ecosystem disturbance history using vegetation
28 demographic models. These models make it feasible to conduct more realistic simulation of
29 processes that control vegetation dynamics. Meanwhile, increasing understanding of the processes
30 governing plant water use, and ecosystem responses to drought in particular, has led to the adoption
31 of dynamic plant water transport (i.e., hydrodynamic) schemes within ESMs. However, the impact
32 of plant hydraulic trait variation in trait-diverse tropical forests is understudied. In this study, we
33 report on a sensitivity analysis of an existing hydrodynamics (HYDRO) model that is updated and
34 incorporated into the Functionally Assembled Terrestrial Ecosystem simulator (FATES). The size
35 and canopy structured representation within FATES is able to simulate how plant size and
36 hydraulic traits affect vegetation dynamics and carbon/water fluxes. To better understand this new
37 model system and its functionality in tropical forest systems in particular, we conducted a global
38 parameter sensitivity analysis at Barro Colorado Island, Panama. We assembled 942 observations
39 of plant hydraulic traits on 306 tropical plant species for stomata, leaves, stems, and roots, and
40 determined the best-fit statistical distribution for each trait, which was used in model parameter
41 sampling to assess the parametric sensitivity. We showed that, for simulated leaf water potential
42 and loss of hydraulic conductivity across different plant organs, the four most important traits were
43 associated with xylem conduit taper (buffers increasing hydraulic resistance with tree height),
44 stomatal sensitivity to leaf water potential, maximum stem hydraulic conductivity, and the
45 partitioning of total hydraulic resistance above vs. belowground. Our analysis of individual
46 ensemble members revealed that trees at a high risk of hydraulic failure and potential tree mortality
47 generally have higher conduit taper, maximum xylem conductivity, stomatal sensitivity to leaf

48 water potential, and lower resistance to xylem embolism for stem and transporting roots. We
49 expect that our results will provide guidance on future modeling studies using plant hydrodynamic
50 models to predict the forest responses to droughts, and future field campaigns that aim to better
51 parameterize plant hydrodynamic models.

52

53
54
55
56
57
58
59
60
61
62
63
64
65
66
67
68
69
70
71
72
73
74

1. Introduction

Tropical forests play a critical role in regulating regional and global climates (Bonan, 2008). Under ongoing and future climate change, they are subjected to substantial risks of climate extremes such as drought and heat waves (Mcdowell et al., 2018). Studies have already shown that tropical forests were experiencing elevated tree mortality rates due to mega droughts related to ENSO events. For example, the 2015–16 El Niño led to the death of an estimated 2.5 ± 0.3 billion stems in the Lower Tapajós river basin of the Amazon and the associated carbon loss had not yet been compensated by new plant growth three years after the event (Berenguer et al., 2021). Such extreme climate events are projected to increase in frequency and intensity under a warming future (Seneviratne et al., 2021). A statistical analysis based on the projection of 13 ESMs under a high greenhouse emission scenario showed that the frequency of extreme droughts as defined by rhizosphere soil moisture (occurring once every 50 years) could increase by a factor of nearly four and this increase would have a disproportionate impact on tropical forests (Xu et al., 2019). The high species diversity found in tropical forests may result in increased resilience to climate extremes, based on the demonstrated resilience of temperate forests in relationship to trait diversity (Anderegg et al., 2018). However, due to limited data to parameterize and constrain models for tropical forests, there is a large uncertainty in our predictive understanding of how tropical forests will respond to these climate extremes (Bonal et al., 2016). This tropical forest uncertainty is a key source of the global uncertainty in projections of land carbon fluxes and future climates (Arora et al., 2020).

75 Earth System Models (ESMs) have been developed to project future changes to the coupled
76 climate and biosphere system. Typically, ‘big leaf’ approximations of vegetation with no
77 explicit presentation of tree size and canopy structure have been used to predict the impact of
78 vegetation on carbon and water cycles. These models do not represent the fundamental
79 elements of vegetation dynamics including growth, mortality, competition, and their response
80 to disturbances. In the last decade, many ESMs have incorporated vegetation demographic
81 models (VDMs) that represent plant size, canopy structure and disturbance histories, with the
82 goal of better representing the competitive dynamics among different size classes of trees and
83 plant functional types in response to climate and disturbances (Fisher et al., 2018). Most of
84 these VDMs can differentiate plants’ light, water and carbon use strategies and can thus
85 represent some part of the functional diversity of tropical forests (Massoud et al., 2019; Koven
86 et al., 2020).

87 Following the ‘big leaf’ model, water limitation on plant gas exchange in these VDMs is
88 generally calculated based on three factors: 1) soil water potential; 2) root distribution; and 3)
89 water potential for stomata openness and closure, all of which differ by plant functional types
90 (Koven et al., 2020). While these soil-moisture-dependent water limitation functions are able
91 to capture trait diversity in leaf-level stomatal behaviors, they fail to capture plant functional
92 diversity in many other observable plant hydraulic traits, such as xylem capacitance, water
93 potentials for loss of xylem hydraulic conductivity, stem hydraulic safety margin, and turgor
94 loss point (Hochberg et al., 2018). Many studies have shown that plant hydraulic traits play an
95 important role in plant responses to droughts (Su et al., 2022; Anderegg et al., 2016), which
96 could shape the landscape distribution of plant functional types (Kunert et al., 2021). In view
97 of this limitation, plant hydrodynamic models have been developed with the aim of better

98 simulating forest response to droughts (Powell et al., 2018; Christoffersen et al., 2016; Xu et
99 al., 2016; Kennedy et al., 2019; Mcdowell et al., 2013). These models not only incorporate
100 hydraulic functional diversity, but also mechanistically simulate the risk of plant mortality due
101 to hydraulic functional failure, as a result of an inability to move water in the xylem due to
102 embolism in conduits (Hammond et al., 2019).

103 One key challenge for these plant hydrodynamic models is that they have many more
104 parameters than simple water limitation functions based on soil water potentials and thus
105 inherently possess more uncertainty in the model parameterization and subsequent simulations.
106 In this study, we describe the implementation of a hydrodynamic scheme within DOE-
107 sponsored functionally assembled terrestrial ecosystem simulator (FATES) (Koven et al.
108 2020), and assess this new configuration with two goals: 1) quantify the parametric sensitivity
109 of different hydraulic traits in determining plant hydrodynamics; and 2) identify key hydraulic
110 traits that are important for predicting the risk of mortality due to hydraulic failure. We expect
111 that our results will provide guidance on model parameterization for future modeling studies
112 using plant hydrodynamic models to predict tropical forest response to droughts, and future
113 field campaigns that aim to collect observational data that can be used to better parameterize
114 and benchmark plant hydrodynamic models.

115 **2. Methodology**

116 **2.1. Model description**

117 We use FATES, a VDM that is coupled within the Energy Exascale Earth System Model
118 (E3SM) (Caldwell et al., 2019). FATES represents size-structured groups of plants (cohorts)
119 and successional trajectory-based patches using the ecosystem demography approach (Fisher
120 et al., 2015; Moorcroft et al., 2001). FATES simulates growth by integrating photosynthesis

121 across different leaf layers for each cohort. FATES allocates this photosynthate to different
122 tissues including leaves, fine and coarse roots, and stem, based on the allometry of different
123 plant functional types, as well as a carbon storage pool (Fisher et al., 2015). Mortality within
124 FATES is simulated by several mechanisms, including carbon starvation caused by depletion
125 of the storage pool, hydraulic function failure, as well as impact mortality during disturbance,
126 fire, logging, freezing, age-related and ‘background’ constant turnover (Fisher et al., 2015;
127 Huang et al., 2020; Fisher et al., 2010; Needham et al., 2020).

128 **2.1.1. Plant Hydrodynamics**

129 The default (non-hydrodynamic) FATES model contains a simplistic algorithm that
130 approximates plant hydraulic failure thresholds based on soil water potential. An important
131 feature of the plant hydrodynamic scheme (HYDRO), which explicitly simulates water flow
132 from the soil through leaves to the atmosphere, is that it enables direct representation of percent
133 loss of conductance as a predictor of hydraulic failure mortality rates. FATES-HYDRO is
134 based on the hydrodynamic model implemented in the Traits-based Forest Simulator (TFS)
135 (Christoffersen et al., 2016) and the features most relevant to the present analysis are
136 summarized below. The model approximates water transport in a single vertical dimension,
137 approximating the canopy as a single leaf layer at the top of a beam, according to the Shinozaki
138 pipe model (Shinozaki et al., 1964) in which the hydraulic path length from the trunk base to
139 each leaf is assumed constant. Following the ‘porous media’ approach, the model simulates
140 the water transport across four main organs (leaves, stem- trunk/branches, transporting roots,
141 and absorbing roots) and different rhizosphere shells (Fig. 1). Resistors connect the different
142 compartments.

143 The water flow is calculated based on water pressure gradients across different
 144 compartments (rhizosphere, absorbing roots, transporting roots, stem, and leaf). Specifically,
 145 flow between compartment i and $i + 1$ (Q_i) is given by,

$$146 \quad Q_i = -K_i \Delta h_i, \quad (1)$$

147 where K_i is the total conductance ($\text{kg MPa}^{-1} \text{s}^{-1}$) at the boundary of compartments i and $i + 1$
 148 and Δh_i is the total matric potential difference between the compartments,

$$149 \quad \Delta h_i = \rho_w g (z_i - z_{i+1}) + (\psi_i - \psi_{i+1}), \quad (2)$$

150 where z_i is compartment elevation difference above (+) or below (-) the soil surface (m), ρ_w
 151 is the density of water (10^3 kg m^{-3}), g is acceleration due to gravity (9.8 m s^{-2}), and ψ_i is
 152 tissue or soil matric water potential (MPa). K_i is treated here as the product of a maximum
 153 boundary conductance between compartments i and $i + 1$ ($K_{max,i}$), and the fractional
 154 maximum hydraulic conductance of the upstream compartments (FMC_i or FMC_{i+1}), which is
 155 a function of the tissue water content as follows,

$$156 \quad FMC_i = \left[1 + \left(\frac{\psi_i}{P_{50,x}} \right)^{a_x} \right]^{-1} \quad (3)$$

157 where ψ_i is the compartmental water potential, $P_{50,x}$ is the water potential at 50% loss of
 158 maximum conductivity for different plant tissues (absorbing root, transporting root, stem), a_x
 159 is the corresponding vulnerability curve shape parameter, with a larger number indicating a
 160 steeper reduction of conductivity in response to more negative water potentials (Choat et al.,
 161 2012). The maximum percentage loss of conductivity (PLC) across different organs [i.e., PLC_i
 162 $= 100 (1 - FMC_i)$] is used to measure the risk of tree mortality (M_{hf}) resulting from hydraulic
 163 failure as follows,

$$164 \quad M_{hf} = M_{hf,base} \frac{\max(0, PLC_{max,organ} - PLC_c)}{100 - PLC_c}, \quad (4)$$

165 where PLC_c is the critical percentage loss of conductivity with risk of mortality, $PLC_{max,organ}$
 166 is the maximum percentage loss of conductivity across different organs, $M_{hf,base}$ is the
 167 baseline mortality rate [fraction/year] when percentage loss of conductivity exceeds PLC_c . In
 168 this version of model, we assume that xylem cavitation can fully recover as long as the trees
 169 do not die.

170 The previous version of this model (TFS-Hydro) presented water in terms of relative water
 171 content (RWC; g H₂O g⁻¹ H₂O at saturation) in line with most empirical work on plant water
 172 relations. While the underlying equations remain unchanged, here we present water in terms
 173 of volumetric water content (θ ; m³ H₂O m⁻³ plant tissue), since this what is accounted by the
 174 model and is consistent with what is tracked in the soil as well. The two quantities are related
 175 via the equation $RWC = \theta / \theta_{sat}$, where θ_{sat} indicates saturated volumetric water content. The
 176 water potential for tissue x [ψ_x] is related to θ_x (the PV curve) following three stages of water
 177 tissue drainage as follows (Tyree and Yang, 1990; Bartlett et al., 2012),

$$178 \quad \psi_x = \begin{cases} \psi_{0,x} + m_{cap} \left(\frac{\theta_x}{\theta_{sat,x}} - 1 \right) & \theta_{ft} < \theta_x \leq \theta_{sat,x} \\ \psi_{sol}(\theta_x) + \psi_p(\theta_x) & \theta_{tlp,x} < \theta_x \leq \theta_{ft,x} \\ \psi_{sol}(\theta_x) & \theta_{r,x} < \theta_x \leq \theta_{tlp,x} \end{cases} \quad (5)$$

179 Stage one applies to stem and roots only and represents the water draw from capillary reserves
 180 (embolized conduits or airspaces in wood) when wood water content is in between full turgor
 181 ($\theta_{ft} = RWC_{ft} \theta_{sat,x}$) and saturation ($\theta_{sat,x}$) and only represents a small fraction of the total
 182 PV curve. It is linear with constant slope $m_{cap} = 11.3 \text{ MPa m}^3 \text{ m}^{-3}$ and $RWC_{ft} = 0.958$ as
 183 estimated from sapwood PV curves on 28 tropical and subtropical species (Christoffersen et
 184 al. 2016). RWC_{ft} is assumed to be 1.0 in leaves. Xylem water potential is assumed zero at full
 185 saturation. The second stage is between full turgor ($\theta_{ft,x}$) and the turgor loss point ($\theta_{tlp,x}$),

186 when the xylem water potential is in balance with solute ($\psi_{sol}[\theta_x]$) and pressure water
 187 potential ($\psi_p[\theta_x]$) of living cells. The third stage is after the turgor loss point ($\theta_{tlp,x}$), but
 188 above the point of residual water content ($\theta_{r,x} = RWC_{r,x} \theta_{sat,x}$) where the water potential is
 189 only a function of the solute water potential. $RWC_{r,x}$ is synonymous with the apoplastic
 190 fraction (Bartlett et al. 2012).

191 The solute water potential is given as,

$$192 \quad \psi_{sol}[\theta_x] = \frac{\pi_0(\theta_{sat,x}RWC_{ft} - \theta_{r,x})}{(\theta_x - \theta_{r,x})}, \quad (6)$$

193 where π_0 is the tissue osmotic potential at full turgor. The pressure potential is calculated as
 194 follows,

$$195 \quad \psi_p[\theta_x] = -|\pi_0| + \varepsilon \frac{(\theta_x - \theta_{sat,x}RWC_{ft})}{(\theta_{sat,x}RWC_{ft} - \theta_{r,x})}, \quad (7)$$

196 where ε is the bulk elastic modulus (MPa).

197 The realized conductivity of the above ground portion of the plant per unit of leaf area (
 198 $K_{l,max,tree,ag}$) is calculated based on xylem hydraulic conductivity at petiole ($k_{s,max,petiole}$),
 199 aboveground tree height (H, meters), and a xylem taper factor (X_{tap}) as follows,

$$200 \quad K_{l,max,tree,ag} = \frac{k_{s,max,petiole}}{H \left(\frac{A_l}{A_s}\right)} X_{tap}, \quad (8)$$

201 where $k_{s,max,x}$ is the maximum xylem conductivity per unit sapwood area, $\frac{A_l}{A_s}$ [i.e., la2sa in
 202 Table 1] is the ratio of leaf area (A_l) to sapwood area (A_s). X_{tap} is the xylem taper factor
 203 representing the ratio of aboveground xylem conductance with taper to that without, which for
 204 intermediate values of conduit taper ($p_taper = 1/6$; see below) represents a factor increase in
 205 total conductance of 23–50 for trees of heights 10–30 meters (Christoffersen et al., 2016).
 206 Savage et al. (2010) highlighted how opposing selective forces will both increase hydraulic

207 conductance by the tapering of conduit radii ($p_taper > 0$) while at the same time protect
 208 against embolism by minimizing conduit taper (no taper implies $p_taper = 0$). They defined
 209 p_taper as the exponent on an external branching parameter (2 daughter branches per parent
 210 branch in their model) that sets the degree of internal branching of xylem conduits (and thus
 211 the tapering of conduit radii as well) and, using a fractal network model, derived an effective
 212 exponent q that describes how aboveground conductance increases with tree size. q is a
 213 monotonically increasing and saturating function of the taper exponent p (see Fig 2b of Savage
 214 et al. 2010); we used this relationship to estimate q , and thus X_{tap} in eq. (8) as

$$215 \quad X_{tap} = \left[\frac{r_{base}}{r_{petiole}} \right]^{q_{tap} - q_{notap}}, \quad (9)$$

216 where r_{base} and $r_{petiole}$ are the trunk and petiole radii, respectively. The ratio $r_{base}/r_{petiole}$ is
 217 related to tree height following the fractal tree model of Savage et al. (2010) (see equations
 218 S12-S13 in Christoffersen et al. 2016).

219 Eq. (8) only gives the aboveground component of whole-plant conductance. In the
 220 absence of a simple first-principles approach to estimating the belowground component, we
 221 estimate the total tree maximum conductance (above- and belowground components) as

$$222 \quad K_{max,tree,total} = R_{frac,stem} K_{max,tree,ag}, \quad (10)$$

223 where $R_{frac,stem}$ is the fraction of total resistance that is aboveground.

224 Stomatal conductance [g_s , $\mu\text{mol m}^{-2} \text{s}^{-1}$] is simulated through a modified Ball-Berry
 225 equation,

$$226 \quad g_s = g_0 + g_1 \frac{A_n}{C_s/P_{atm}} h_s, \quad (11)$$

227 where g_1 is the stomatal conductance slope in response to environmental condition changes,
 228 g_0 is the minimum (cuticular) stomatal conductance ($\mu\text{mol m}^{-2} \text{s}^{-1}$), C_s is the leaf surface CO_2

229 partial pressure (Pa), P_{atm} is the atmospheric pressure (Pa), h_s is the leaf surface humidity,
 230 and A_n is leaf net photosynthesis rate ($\mu\text{mol CO}_2 \text{ m}^{-2} \text{ s}^{-1}$). Stomatal conductance is further
 231 modified by a plant water stress factor, β , calculated as

$$232 \quad \beta = \left[1 - \left(\frac{\psi_{leaf}}{P_{50,gs}} \right)^{a_{gs}} \right]^{-1}, \quad (12)$$

233 where ψ_{leaf} is the leaf water potential, $P_{50,gs}$ is leaf water potential at 50% loss of maximum
 234 stomatal conductance, and a_{gs} is the stomatal vulnerability shape parameter.

235 The total fine root surface area affects the amount of water a plant can take up through its
 236 influence on rhizosphere conductance and is determined by both the specific root length (srl)
 237 and absorbing root radius (r_{s2}). Specifically, the model has a specified number of soil shells
 238 (5 in this study) around fine root surfaces and the conductance between soil shell $k+1$ and k ,
 239 $K_{shell,k}$, is calculated as,

$$240 \quad K_{shell,k} = K_s \frac{\pi l_{aroot,common}}{\ln(r_{k+1}/r_k)}, \quad (13)$$

241 where r_k is the mean radi of k th shell, $l_{aroot,common}$ is the total length of absorbing roots
 242 calculated as a product of total fine root biomass and specific root length (srl). K_s is set to be
 243 the conductance for soil (K_{soil}) when $k>1$. For $k = 1$,

$$244 \quad K_s = \frac{1}{\frac{1}{K_{soil}} + \frac{1}{K_{root,soil}}}, \quad (14)$$

245 where $K_{root,soil}$ is the conductance between fine root surface and soil. An update to the TFS-
 246 Hydro approach is to make this conductance direction-specific, in view that water loss rate
 247 from root could be substantially lower than water uptake rate either through osmotic regulation
 248 (Dichio et al., 2006) or by lacunae caused by rupture of cortical cells (North and Nobel, 1992)
 249 during drought. It is determined by either the maximum uptake of water per unit of absorbing
 250 root surface area ($k_{r1,max}$, $\text{kg m}^{-1} \text{ s}^{-1} \text{ MPa}^{-1}$) when root water potential is more negative than

251 adjacent rhizosphere soil water potential, or the maximum root water loss rate per unit surface
252 area ($k_{r2,max}$, $\text{kg m}^{-1} \text{s}^{-1} \text{MPa}^{-1}$) when rhizosphere water potential becomes more negative than
253 root water potential, which may occur, for example, in frozen soils or in very dry soil layers
254 (Schmidhalter, 1997).

255 The plant hydrodynamic representation and numerical solver scheme within FATES-
256 HYDRO follows the 1-D solver laid out by Christoffersen et al. (2016), which is the default
257 solver in FATES-HYDRO and used in this study. The model also has an option of a 2-D solver,
258 which is slower and detailed by Fang et al. (2022) and Lambert et al. (2022). The equations
259 are solved for tissue water content at a 30 minutes time step. We made a few modifications to
260 accommodate multiple soil layers and improve the numerical stability. First, to accommodate
261 the multiple-soil layers, we sequentially solve the Richards' equation for each individual soil
262 layer, with each layer-specific solution proportional to each layer's contribution to the total
263 root-soil conductance. Second, to improve the numerical stability, we now linearly interpolate
264 the pressure/volume curve beyond the residual and saturated tissue water content to avoid the
265 rare cases of overshooting in the numerical scheme under very dry or wet conditions. See the
266 Supplementary Information [HYDRO_DESCRIPTION.pdf] for further details of the
267 implementation.

268 **2.1.2. Non-hydrodynamics processes**

269 FATES-HYDRO can be coupled to different host land models (HLMs) including the
270 E3SM land model (ELM) (Caldwell et al., 2019) or the Community Terrestrial Systems Model
271 (CTSM) (Lawrence et al., 2019). In this study, the model is coupled to ELM. In this section,
272 we layout the key non-hydrodynamic processes in the FATES or the ELM for a better
273 understanding of parameter importance in the results.

274 Canopy radiative transfer is calculated using a multi-layer scheme based on the iterative
275 Norman radiation scheme (Norman, 1979). Leaf and stem area is binned into a matrix of
276 canopy layer, leaf layer and plant functional types. Reflectance, absorption, and transmittance
277 are calculated for each leaf layer. Between canopy layers, light streams are averaged between
278 plant functional types (PFTs), such that all PFTs in understory layers receive equal radiation
279 on their top leaf layer. Fractional absorption of visible and near infra-red light is calculated
280 separately for direct and diffuse light. For the direct stream, transmitted and reflected light is
281 converted into diffuse fluxes. In FATES, the absorbed PAR is used to calculate photosynthesis
282 rates for each of the canopy layer x leaf layer x PFT bins, after which rates across layers are
283 re-aggregated into cohort level carbon fluxes. Please see the Supplementary file in Fisher et al.
284 (2015) for details.

285 The energy balance is handled by the host land model. In this study, it is based on the land
286 component of DOE's Exascale Energy Earth System Model (E3SM). The E3SM land model
287 (ELM) is based on the Community Land Model 4.5 (Oleson, 2013). Specifically, in ELM, the
288 average canopy temperature is calculated based on the energy balance of latent heat, sensible
289 heat, and absorbed radiation as determined by the radiative transfer model. The latent heat is
290 determined by the transpiration, which is determined by the vapor pressure deficit from inside
291 of leaf to the air, canopy stomatal conductance, and boundary layer conductance. FATES
292 calculated mean canopy stomatal conductance averaged across different cohorts, which is fed
293 to ELM to calculate the energy balance. The Newton-Raphson numerical scheme is used to
294 solve for the canopy temperature.

295 All aspects of soil water balance (infiltration, water transfer among soil layers, and
296 drainage) happen at the 'column' scale at 30-min time steps and are handled within the Host

297 Land Model (see Oleson et al. 2013 for a detailed description of hydrology in CLM4.5, the
298 parent model of ELM). FATES-HYDRO handles soil water operations at the patch and cohort
299 scales. It simulates root water uptake and changes in plant water potential from roots to leaves
300 based on current time step transpiration. The belowground conductance for each soil layer is
301 weighted by root biomass with an exponential vertical distribution. Sections 2 and 3 in the
302 Supplement of this manuscript provide full details on boundary conditions, sequence of
303 operations among HYDRO and the HLM, downscaling of soil moisture to rhizosphere shells,
304 and downscaling of transpiration from the patch to individual scale.

305 **2.2. Sensitivity analysis**

306 We identified 35 parameters for the FATES-HYDRO model to conduct the parametric
307 sensitivity analysis (Table 1). To estimate the parameter distributions, we started with
308 published meta-analyses (Christoffersen et al., 2016; Choat et al., 2012; Bartlett et al., 2012;
309 Bartlett et al., 2014; Bartlett et al., 2016; Klein, 2014) and supplemented them with select new
310 data from individual studies. Focal data were tissue- or individual-level hydraulic traits
311 spanning water transport and embolism resistance, tissue water storage and retention (PV curve
312 traits), hydraulic architecture (i.e., leaf area to sapwood area ratio), stomatal responses to
313 dehydration, and fine root traits (Table 1). For each dataset, we standardized taxonomic names
314 using the TNRS package in R (Boyle et al., 2013). This allowed us to join datasets together
315 based on species, averaging multiple observations per species if necessary, resulting in a
316 species-specific sparse matrix of all hydraulic traits for all databases and individual studies that
317 we compiled. This pantropical hydraulic trait dataset is included in the Supporting Information
318 [traits_master_trop.csv].

319

320 This trait dataset consisted of anywhere from 1 - 323 observations for each trait, where
321 each observation corresponds to a different species (multiple observations for the same species
322 are first averaged; see above). Before fitting distributions to these data, some traits were first
323 transformed to be positive (e.g., P50) or normalized within [0, 1] when upper and lower bounds
324 were well-defined (Table 1). Then, for each trait separately, we used the `fitdistr` package in R
325 to estimate best-fit parameters for uniform, beta, normal, lognormal, and gamma statistical
326 distributions in order to estimate central tendencies and spread for each trait. The distribution
327 with the largest log likelihood and best-fit parameters are given in Table 1. Each model
328 simulation consisted of a single PFT: all trees (across all cohort sizes and patches) had the
329 same traits.

330 We augmented observations with extratropical data to increase sample size for traits with
331 less than three tropics-specific observations. When trait data observations were not present, we
332 used a uniform distribution bounded on our best estimate of the theoretical range (Table 1).
333 As there is limited data on roots, we used the same distribution as that for branches if data were
334 lacking. Because our goal is to understand the model behaviors as determined by different
335 hydraulic traits, we assumed independence among traits. As we focused on the hydraulic traits
336 in this study, we used non-hydraulic trait values based on an optimal set of parameters that best
337 fit observed water and carbon fluxes in a set of FATES simulations run without hydrodynamics
338 (Koven et al., 2020).

339 We used the Fourier Amplitude Sensitivity Test (FAST) to assess the relative importance
340 of parameters in determining the variance of model outputs (Xu and Gertner, 2011a). The main
341 idea of FAST is to assign periodic signals in the sampled parameter values and use Fourier
342 transformation to identify the signals in the outputs. Sampled parameter values are based on

343 Latin hypercube sampling from the fitted statistical distributions (see previous section for more
344 details). We ran 1000 ensemble simulations of the FATES-Hydro to derive model outputs of
345 water potential and fraction of maximum conductivity. For each ensemble simulation, each
346 plant hydraulic trait was assigned with a random draw from each trait's distribution, and the
347 samples for different traits are randomly combined to sample the observed plant hydraulic trait
348 space for sensitivity analysis.

349 We used the Uncertainty Analysis and Sensitivity Analysis (UASA) tool
350 (<https://sites.google.com/site/xuchongang/uasatoolbox>) to estimate the parametric sensitivity
351 index, which is calculated based on the ratio of the partial variance in the model output
352 attributed to a specific parameter to the total variables in the model output. For details, please
353 refer to Xu and Gertner (2011a). We ran the model with 1000 ensemble members, in view that
354 an order of 100 times effective important number of parameters, which we estimate to be ~10,
355 is needed to achieve reasonable precision (Xu and Gertner, 2011b).

356 **2.3. Study area**

357 In this study, we used Barro Colorado Island (BCI), Panama, as our test site to evaluate
358 model behavior. We chose BCI because it has moderately strong dry and wet seasons that
359 allow us to assess the hydrodynamics under different levels of water availability. Moreover,
360 extensive field campaigns in recent years have provided comprehensive data needed for model
361 parameterization, initialization and climate drivers. Finally, we also leverage prior FATES
362 studies of non-hydraulic parameters at BCI (Koven et al., 2020).

363 BCI has an annual mean temperature of 26.3°C and an annual mean precipitation of 2656
364 mm with a strong seasonal precipitation signal. The dry season lasts from January to April,
365 with a mean precipitation of 228mm, while the wet season lasts from May-December with a

366 mean precipitation of 2428mm (Paton, 2020). In this study, we used hourly in-situ climate data
367 from 2008-2016 to drive the model. To run the model to equilibrium (in terms of soil moisture
368 content) takes 5-6 years, thus we choose February of 2016 as the target for analysis of dry
369 season hydrodynamics and August of 2016 as the target for analysis of wet season
370 hydrodynamics.

371 **2.4. Model setup**

372 In this study, as our focus is on the plant hydrodynamics, we used the static stand structure
373 mode of FATES that turns off the processes of competition, growth and mortality, to instead
374 hold the ecosystem structure constant. This reduced-complexity configuration (Fisher and
375 Koven, 2020) thus exercises only the primarily fast-timescale-processes of photosynthesis,
376 transpiration, water transport, and plant hydrodynamics (i.e., change in hydraulic conductivity,
377 water storage, and water potentials in plant tissues). By using static stand structure mode, as in
378 Chitra-Tarak et al. (2021), we isolate hydraulic trait controls on simulated hydrodynamics and
379 avoid confounding, and potentially biased, feedbacks from resulting changes in forest
380 structure. Using static stand structure mode also means that we do not need to spin up
381 vegetation state, thus reducing the simulation time. The forest stand structure, consisting of
382 tree size and composition for each patch, is initialized based on forest inventory data collected
383 in 2015 (<http://ctfs.si.edu/webatlas/datasets/bci/>). As the majority of species in BCI are
384 evergreen broad leaf trees, we ran the model with one PFT with different hydraulic traits (Table
385 1) to assess their impact on the hydrodynamically relevant outputs including water potentials
386 and fraction of maximum conductivity for different plant organs including absorbing root,
387 transporting root, stem, and leaves.

388 One key benefit of utilizing a hydrodynamic model is its ability to simulate the risk of
389 hydraulic failure by considering the loss of conductivity in various plant organs. As FATES
390 model was ran on static stand mode, we did not specifically simulate the tree mortality resulting
391 from the hydraulic failure as shown in Eq. (4). Instead, we used the maximum of loss of
392 conductance across the continuum of plant nodes [i.e., $PLC_{max,organ}$ in eq. (4)] to assess the
393 hydraulic failure risk. If $PLC_{max,organ}$ reaches critical threshold PLC_c , which is set to 50%
394 (Adams et al., 2017), trees are assumed to be faced with a high risk of mortality. Using the
395 ensemble simulations, we also aim to identify the most vulnerable plant organs and the critical
396 parameters that influence the likelihood of hydraulic failure.

397 FATES simulates the carbon and water fluxes for different size classes of trees. The forest
398 has 137 cohorts with diameters ranging from 10 cm to >2 meters and height ranging from 1 to
399 38 meters (see Fig. S1 for size distributions). Because large trees experience more fluctuations
400 in environmental conditions in the canopy and higher risk of mortality due to drought (Bennett
401 et al., 2015), we focused on hydrodynamic behaviors for large trees with diameter at breast
402 height (DBH) more than 60 cm; however, for comparison, we also derived the sensitivity for
403 smaller trees with DBH less than 60 cm.

404 3. Results

405 Our results showed that the simulated ranges across the ensemble of leaf water potential
406 (Fig. 2) and loss of conductivity (Fig. 3) are large. For leaf water potential of large trees with
407 diameter > 60 cm, the 95% percentile ranges are from -5 MPa to -0.5 MPa and -3 MPa to -0.5
408 MPa for February (dry) and August (wet) 2016, respectively. Correspondingly, the fraction of
409 maximum stem hydraulic conductivity is much higher during August compared to February
410 (Fig. 3); however, in both months, the modeled range spans almost the full range of between 0

411 and 1. For smaller trees with diameter less than 60 cm, our results show that smaller tree
412 experienced less negative water potential (Fig. S2 and Fig. 2) and lower loss of hydraulic
413 conductivity (Fig. S3 and Fig. 3).

414 Based on the FAST sensitivity indices (i.e., the variance in model output contributed by
415 different parameters), the key parameters that control the water potentials of different plant
416 organs (leaf, stem and root) for large trees (diameter >60 cm) include the taper exponent for
417 hydraulic conductivity (p_taper), the water potential leading to 50% loss of stomatal
418 conductance ($p50_gs$), maximum hydraulic conductivity for the stem ($kmax_node_stem$), and
419 the fraction of total hydraulic resistance in the above ground section ($rfrac_stem$), in decreasing
420 order (Fig. 4). For the fractional loss of conductivity, the most important parameter is the water
421 potential leading to 50% loss of hydraulic conductance (P_{50}) for the corresponding organs (Fig.
422 5). Other important parameters are similar to those for simulated water potentials. Notably, the
423 organ-specific P_{50} values are more important for the dry month (February) compared to the
424 wet month (August). For the wet month of August, p_taper is the dominant parameter
425 controlling the pre-dawn and midday loss of hydraulic conductivity, while organ-specific P_{50}
426 parameters are the second most important. For smaller trees with diameter less than 60 cm, the
427 corresponding parametric sensitivity patterns are similar to those of larger trees (Fig. S4 and
428 Fig. S5); however, compared to larger trees, the parametric sensitivity of p_taper for simulated
429 leaf water potential becomes lower for smaller trees (Fig. 4 and Fig. S4).

430 In terms of the risk of hydraulic failure, out of the 1000 ensemble members, ~40% of the
431 simulations for February and ~60% of simulation for August suggest that branches are the most
432 vulnerable plant organ, based on highest loss of conductivity across the continuum from root
433 to branch (Fig. 6). For the dry month of February, roots are at greater risk in comparison to the

434 wet season. If we consider the loss of conductivity more than 50% for February 2016 as a
435 threshold for a high risk of mortality (Adams et al., 2017), then 53% of ensemble simulations
436 reach this threshold. The key parameters affecting the risk of mortality, as measured by
437 percentage difference in parameter values for ensemble members reaching 50% loss of
438 conductivity or not, include the water potential leading to 50% loss of conductance for stomata
439 ($p50_gs$), stem ($p50_node_stem$), and transporting roots ($p50_node_root$), maximum
440 hydraulic conductivity of stem ($kmax_node_stem$), and the taper exponent (p_taper) (Fig. 7).
441 Ensemble members with high risk of mortality generally have a higher p_taper and
442 $kmax_node_stem$, less negative $p50_gs$, and less negative $p50$ for stem and transporting roots
443 (Fig. 8).

444 **4. Discussion**

445 Our analysis showed the importance of key plant hydraulic traits in simulating plant water
446 potential and risk of hydraulic failure. This analysis identifies these parameters as potential
447 targets of either model calibration or targeted measurement campaigns to achieve realistic
448 simulations. In our sensitivity analysis, the most influential parameter for both water potential
449 and loss of conductivity is the tapering of the radius of conduit with increasing plant height
450 (p_taper). As p_taper increases, the conduit radius increases from the top of the tree to its
451 base. According to Hagen-Poiseuille's equation, this increases the theoretical maximum total
452 conductance. Low values of p_taper thus limit the adverse effects of tree height by increasing
453 k_max along the whole continuum and reducing the soil-to-leaf water potential needed to
454 maintain transpiration. Our inference is that p_taper represents an overarching property of
455 plant architecture that influences the relative effect of each of the other traits related to
456 hydraulic safety and efficiency (Olson et al., 2021). The xylem architecture as determined by

457 *p_taper* parameter could change in response to age and development stages (Rodriguez-
458 Zaccaro et al., 2019), which is not considered in this study. Future studies evaluating the
459 importance of this change to hydraulic functions could be useful to guide size-dependent
460 growth and mortality. Another dimension of the hydraulic architecture with a critical role in
461 determining both water potential and loss of conductivity, though to a much lesser degree, was
462 the fraction of total tree resistance that is belowground (i.e., of the entire transporting and
463 absorbing root system; $1 - rfrac_stem$). Generally, a plant will match the growth of its trunk
464 and crown to maintain a degree of equilibrium in aboveground resistance as the distance water
465 needs to travel increases (Yang and Tyree, 1993). In this study, due to the lack of data on the
466 belowground resistance, we assigned a quite large range for this trait, which could be impacted
467 by many factors such as belowground root biomass, root network architecture, and interactions
468 between roots, fungi and bacteria (Poudel et al., 2021; Bhagat et al., 2021).

469 The second most sensitive parameter in determining loss of conductance was the leaf water
470 potential at 50% loss of stomatal conductance (*p50_gs*). This parameter controls the water loss
471 rate from leaves, with a less negative value providing protection from hydraulic failure during
472 water-limited periods. The *p50_gs* trait has been shown to play a key role in tree survival
473 during severe droughts (Breshears et al., 2009; Rowland et al., 2015). The ability to withstand
474 lower leaf water potentials is also a key indicator of sapling and seedling survival during
475 drought and determines species distribution across a moisture gradient (Kursar et al., 2009).
476 There may be a trade-off between drought tolerance (with a lower *p50_gs*) and drought
477 avoidance (a less negative *p50_gs* but with a high capacitance; the amount of water released
478 from reserves as leaf water potential declines), a crucial aspect in determining species drought
479 resistance (Pineda-Garcia et al., 2013). Additionally, loss of conductivity was sensitive to the

480 water potential at 50% loss of max conductivity within the stem (*p50_stem*) as it can largely
481 affect the whole plant conductance and thus the water supply to the leaves. *p50_stem*
482 negatively correlates with wood density and may be a marker of the trade-off between
483 hydraulic efficiency and safety within the stem (Chen et al., 2009; Manzoni et al., 2013);
484 however, other studies have shown that this trade-off is weak (Gleason et al., 2016). Liang et
485 al (2019) showed that the strength of this trade-off could be dependent on specie's drought
486 strategies.

487 Leaf water potential and loss of conductance were both sensitive to the maximum xylem
488 conductivity in the stem (*kmax_node_stem*). Higher maximum conductivity represents greater
489 xylem efficiency, which in the absence of drought or light limitations would result in greater
490 potential photosynthesis and less negative water potentials (Gleason et al., 2016). However,
491 xylem with higher *kmax_node_stem* could be more vulnerable to embolism as water potential
492 declines (Sperry and Love, 2015). In tropical rainforests, species with higher conductivity per
493 unit leaf area generally are less desiccation-tolerant, and thus exhibit higher mortality rates
494 (Kursar et al., 2009). Low *kmax_node_stem* along with high leaf-to-sapwood area ratio (*la2sa*)
495 also represents a vulnerability to reduced conductance which increases with height
496 (Christoffersen et al., 2016).

497 Traits with lower order of impacts on water potential modulate the amount of stored water
498 available during drought. The bulk modulus of elasticity in the root (*epsil_node_aroot*)
499 together with root saturated water content determines the amount of water available from
500 cellular storage between complete hydration and loss of turgor (Powell et al., 2017). This
501 represents the ability of the roots to continually supply water to the rest of the plant as drought
502 occurs. It also represents an investment in cellular structure, which may be an additional

503 indicator of adaptations with non-hydraulic origin. The residual water content in the stem
504 (*resid_node_stem*) determines the minimum amount of water xylem will hold and thus impact
505 the amount of water storage plant can use during drought as well (Bartlett et al. 2012). In this
506 study, we made the assumption that the traits are independent of each other, in order to
507 understand the hydrodynamic behaviors of FATES-HYDRO for different hydraulic traits
508 based on a single PFT. Understanding the trade-offs between these traits is crucial for
509 determining the competition among different PFTs. Future studies would greatly benefit from
510 assessing the significance of these trade-offs to predict vegetation dynamics under future
511 climate change.

512 In contrast to the majority of hydraulic traits in the model, conduit taper, the fraction of
513 total resistance belowground, and the leaf to sapwood area ratio are whole-plant hydraulic
514 traits. Our analysis highlights the importance of whole-plant hydraulic traits such as conduit
515 taper relative to tissue-level hydraulic traits for a range of plant hydraulic functions, including
516 whole-plant conductance and hydraulic failure risks. An important area for future work is to
517 better constrain and understand the consequences of intra- and interspecific variation in these
518 whole-plant hydraulic traits in tropical forests. Our choice of the range of variation in the
519 conduit taper exponent came from a study on temperate species, and was broad, encompassing
520 the entire range of observed values in that study (Savage et al. 2010). Further, we estimated
521 the effects of variation in the taper exponent on whole-plant conductance conditional on trees
522 following a simple set of optimality assumptions (space-filling, area-conserving, and self-
523 similar branching network structure). However, in practice, such assumptions are often not met
524 (Smith et al., 2014). Therefore, it is possible that the model sensitivity to xylem taper in terms
525 of whole-plant hydraulic function are overestimated. Nevertheless, our study highlights the

526 importance of better constraining this parameter as well as further experimentation with
527 alternate model structures to better account for non-optimal trees in tropical forests.

528 The sensitivity of vegetation to drought stress and hydraulic-failure-induced mortality is of
529 paramount importance for understanding how ecosystems may respond to shifting temperature
530 and rainfall patterns under a changing climate (Mcdowell et al., 2022). We recognize that
531 parametric sensitivity could be different for different sites depending on climate driver, soil
532 moisture and vegetation types. However, we expect the main parameter of importance could
533 be useful to guide model calibration to select the candidate parameters for different sites. As
534 understanding of plant hydrodynamics increases, linking model predictions to observable plant
535 traits has emerged as a promising means of constraining predictions of ecosystem resilience.
536 Such traits are challenging and costly to measure in the field and thus resources must be
537 directed carefully when planning measurement campaigns. The identified parameters in this
538 study could provide guidance on the limited measurement we could target in the field.

539 **5. Acknowledgment**

540 This research was supported as part of the Next Generation Ecosystem Experiments-
541 Tropics, funded by the U.S. Department of Energy, Office of Science, Office of Biological and
542 Environmental Research. RF acknowledges funding by the European Union’s Horizon 2020
543 (H2020) research and innovation program under Grant Agreement No. 101003536 (ESM2025
544 – Earth System Models for the Future) and 821003 (4C, Climate-Carbon Interactions in the
545 Coming Century).

546 **6. CODE and Data Availability**

547 The FATES-HYDRO code is available from <https://doi.org/10.5281/zenodo.7686333>. The
548 traits data are in the supplementary file [traits_master_trop.csv].

549 **7. Supplement Information**

550 Three supplementary file are included. The HYDRO_DESCRIPTION.pdf provide the
551 summary of the hydrodynamic implementation that is different from Christoffersen et al.
552 (2016). The traits_master_trop.csv file include all the hydraulic traits we assembled for the
553 tropical region. The supplementary_figure.pdf provides additional figures for the main text.

554 **8. Author contribution**

555 CX and BC designed the sensitivity analysis experiments. BC collected the data and fitted
556 the trait distributions. CX conducted the analysis and drafted the manuscript. BC, CX, RF, RN
557 and CK designed the implementation of HYDRO codes. BC implemented the majority of
558 HYDRO codes with code improvement made by CX and RN. ZR conducted the ensemble
559 model simulations. MS provided the leaf cuticular conductance data. NM, CK and LK
560 provided guidance on the sensitivity analysis, code development and trait data synthesis. All
561 authors contributed to manuscript writing by providing edits and suggestions.

562 **9. Competing interests**

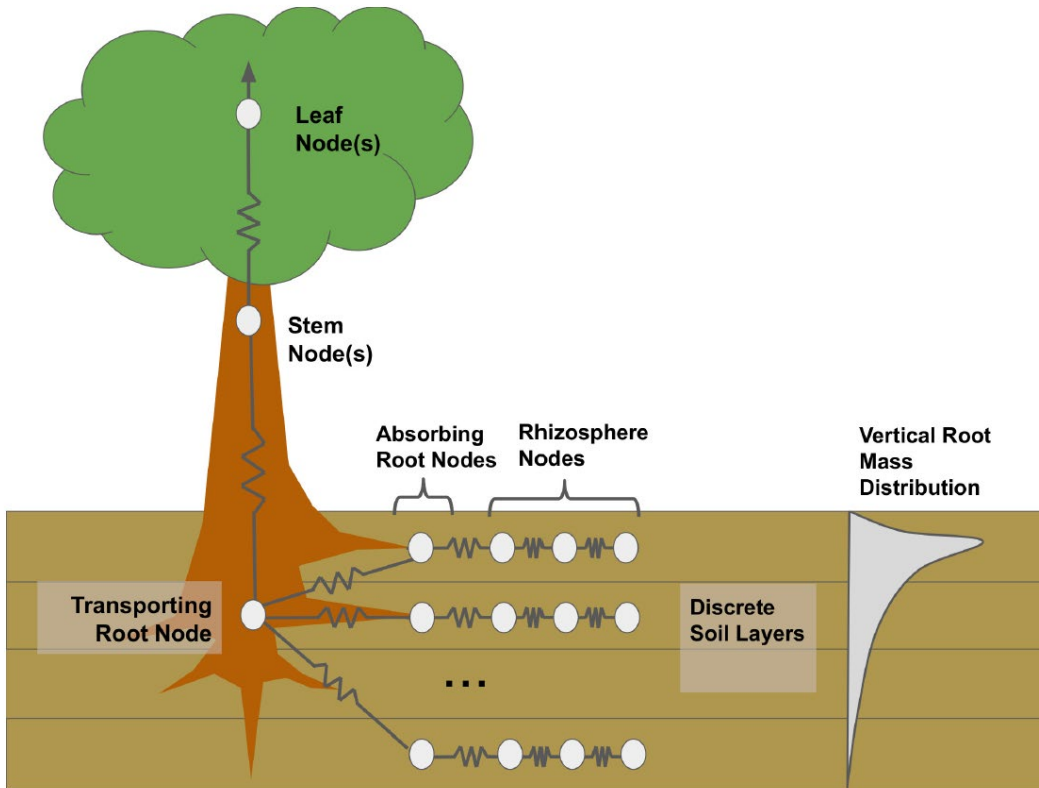
563 The contact author has declared that none of the authors has any competing interests.

564

565

566 **Figures**

567



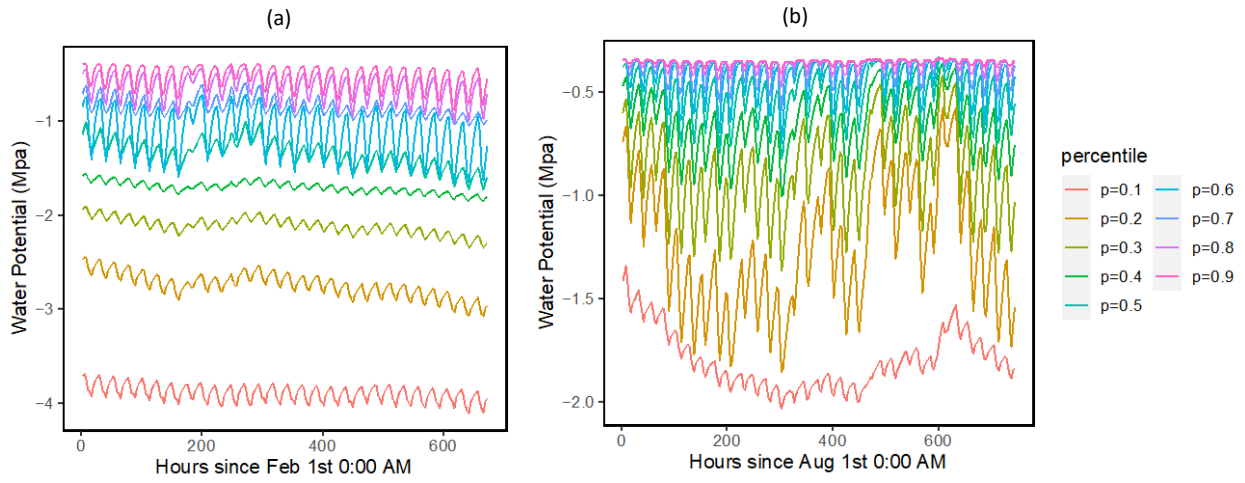
568

569 **Figure 1: Diagram of FATES-HYDO with simulation of rhizosphere shell, absorbing roots, transporting roots, stem and**

570 **leaves. The model is solved for different soil layers with different root distributions.**

571

572



573

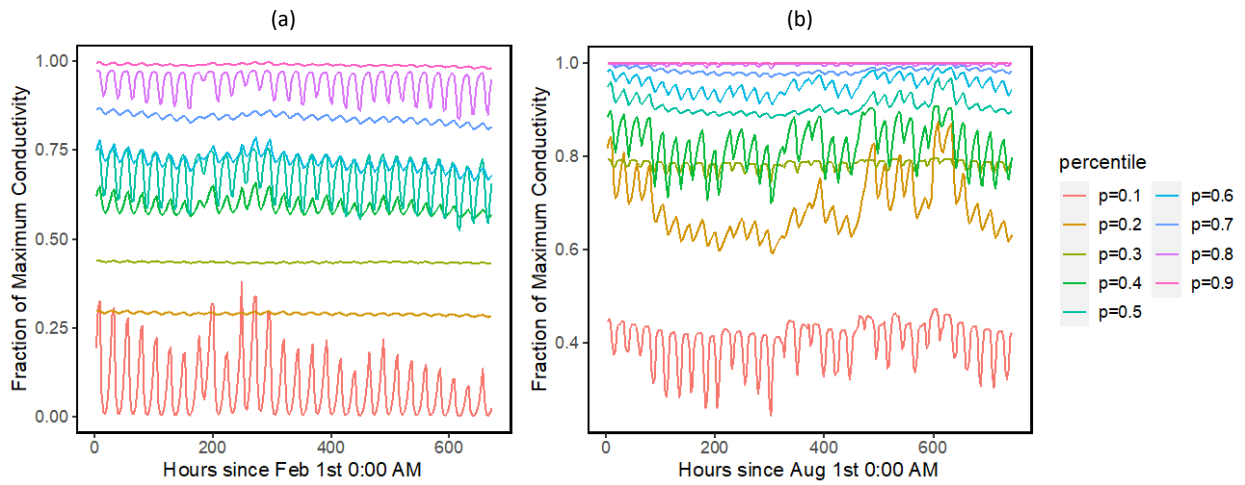
574

575 **Figure 2: Simulated ranges of leaf water potential for February (a) and August (a), 2016 for trees with DBH > 60cm. The**

576 **percentiles are calculated based on the monthly mean values of leaf water potentials for the 1000 ensemble simulations.**

577

578



579

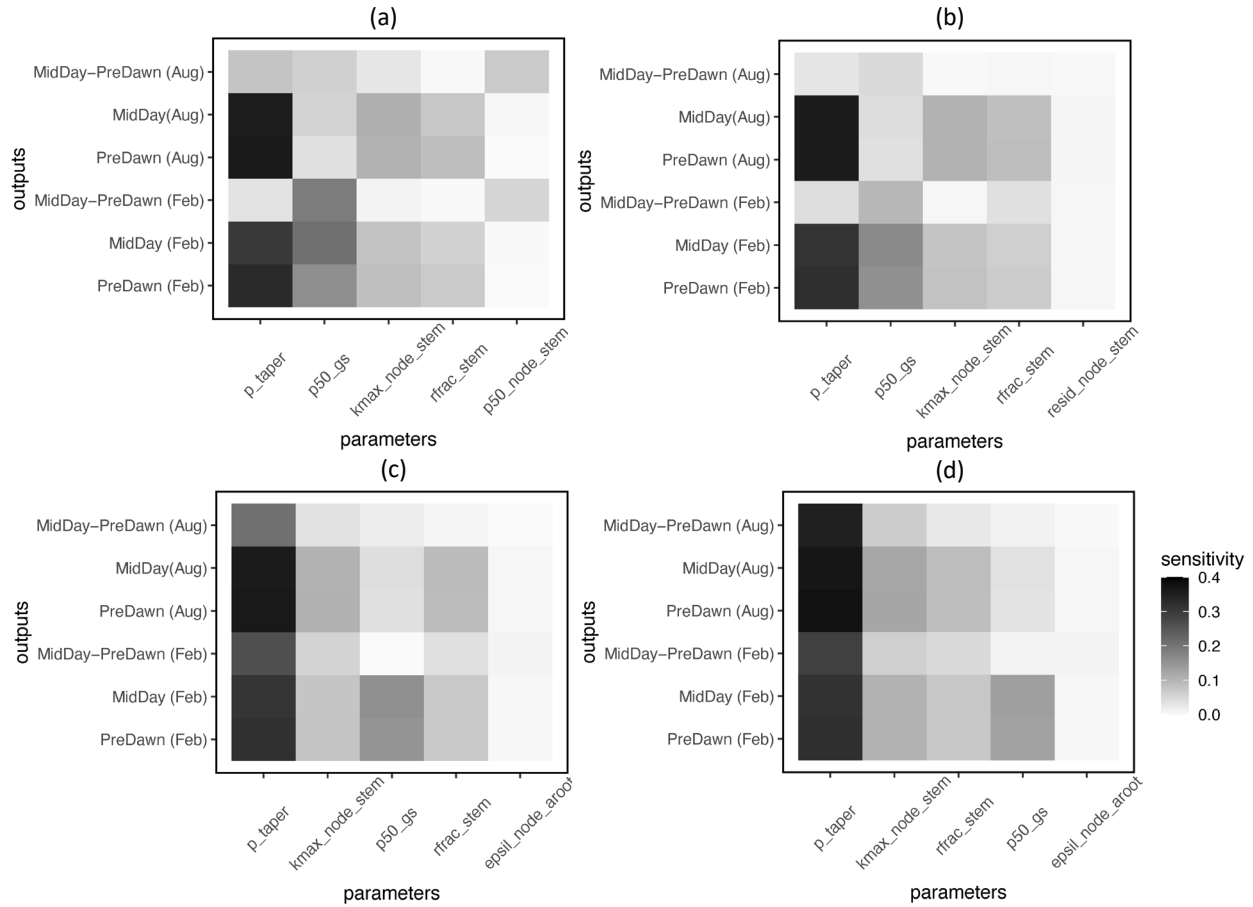
580 **Figure 3: Simulated ranges of fraction of maximum hydraulic conductivity of stem for February (a) and August (a), 2016**

581 **for trees with DBH > 60cm.** The percentiles are calculated based on the monthly mean values of leaf water potentials for the

582 1000 ensemble simulations.

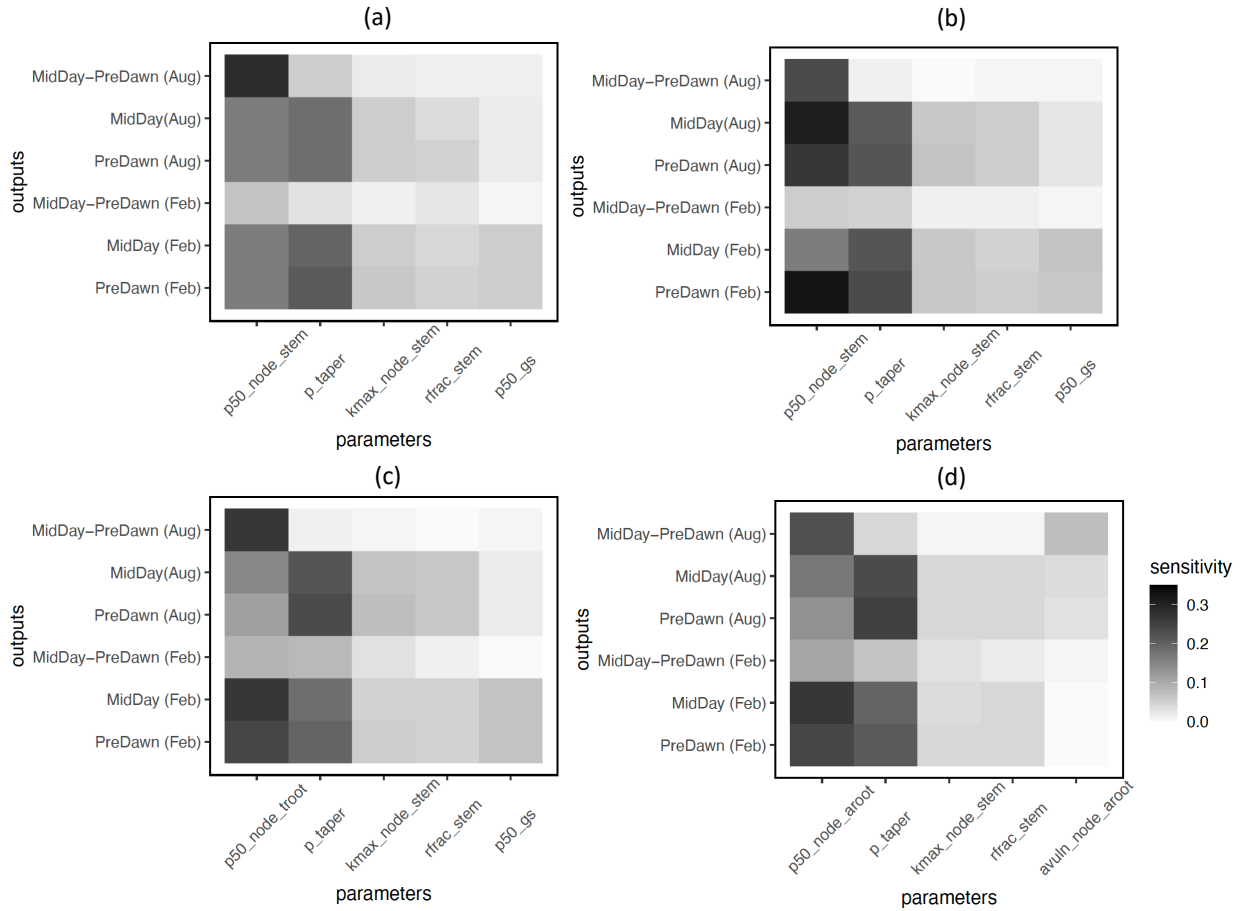
583

584



585
 586 **Figure 4: Key parameters that control simulated water potentials for leaf (a), stem (b), transporting root (c) and**
 587 **absorbing root (d), for trees with DBH > 60cm.** The sensitivity value refers to the proportion of total model output variance
 588 contributed by a specific parameter (0-1). See Table 1 for the explanation of the parameters.

589



590

591

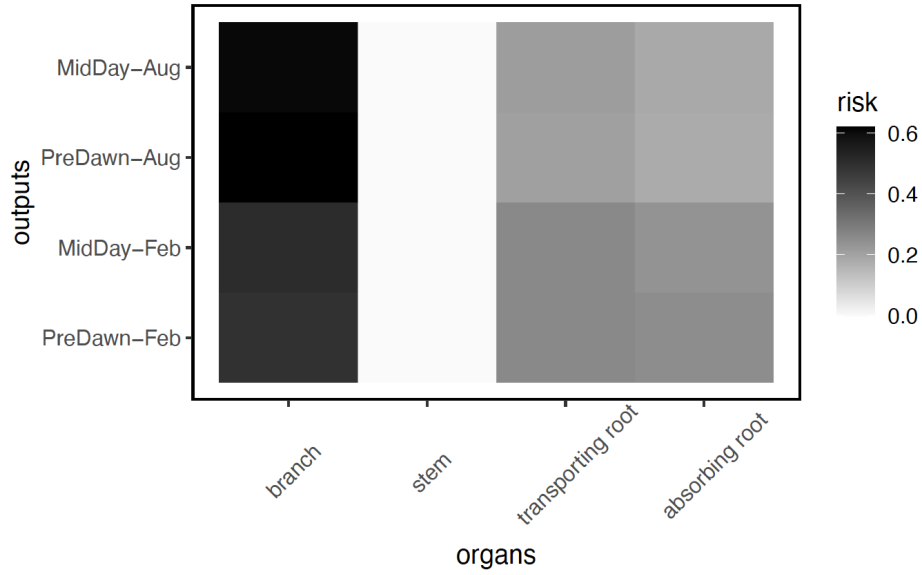
592 **Figure 5: Key parameters that control simulated loss of conductivity for branch (a), stem (b), transporting root (c) and**

593 **absorbing root (d), for trees with DBH > 60cm. The sensitivity value refers to the proportion of total model output variance**

594 **contributed by a specific parameter. See Table 1 for the explanation of the parameters. See Table 1 for the description of**

595 **parameters.**

596



597

598

599

600

601

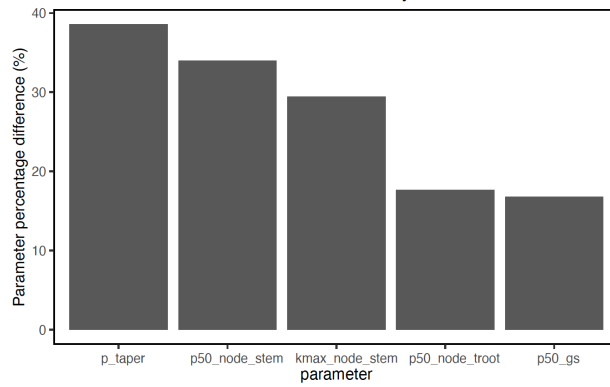
602

Figure 6: Risk on the continuum for hydraulic failure as measured by percentage of total number of simulations with highest loss of conductivity for a specific organ (branch, stem, transporting root and absorbing root), for trees with DBH > 60cm. As the model does not specifically simulate the branch, we calculated the risk of loss of conductivity based on the leaf water potential and hydraulic vulnerability curve from xylem.

603

604

605



606

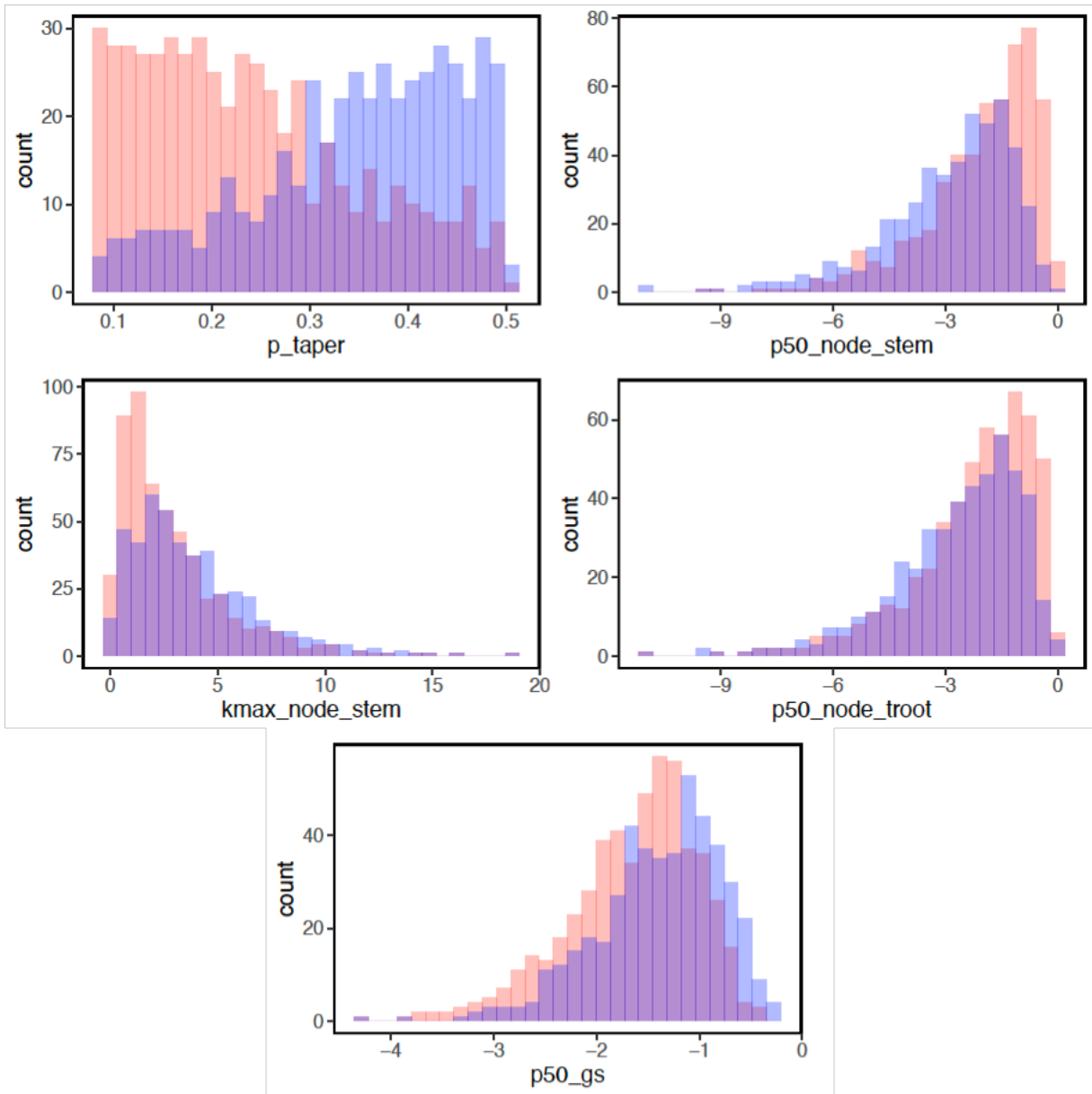
607 **Figure 7: Mean trait percentage difference for model ensemble simulations with loss of hydraulic conductivity larger**

608 **than 50% and ensemble simulations with loss of hydraulic conductivity less than 50%, for trees with DBH > 60cm. See**

609 Table 1 for the description of parameters.

610

611



612

613 **Figure 8: Parameter difference for ensemble members with risk of mortality, for trees with DBH > 60cm.** Blue bars
 614 indicate parameter values with lower mortality risk (<50% loss of hydraulic conductivity). Red bars indicate parameter values
 615 with higher mortality risk (>= 50% loss of hydraulic conductivity) and purple bars indicate parameter values stacked from
 616 transparent red/blue bars. See Table 1 for the description of parameters.

617

618

Table 1 Hydraulic parameters considered in the sensitivity analysis

| PARAMETER (EQUATION NUMBER) | SYMBOL | UNITS | DISTRIBUTION ¹ | SOURCES& NOTES |
|--|------------------|---|--|--|
| Pressure-Volume (PV) curve (water content – water potential relationship) | | | | |
| saturated water content (thetas_node) (Eq. 5) | $\theta_{sat,x}$ | cm ³ cm ⁻³ | Leaf: Beta (9.69, 6.20) Stem: Beta (12.67, 7.4626) TRoot and AROOT: Beta (22.98, 5.29) | Christoffersen et al. (2016) Iversen et al. (2017) Wright et al. (2010) Roderick et al. (1999) Sack et al. (2003) Binks et al. (2016) |
| turgor loss point (tlp_node) (Eq. 5) | π_{tlp} | MPa | $\pi_{tlp} = (\pi_0 \epsilon) / (\pi_0 + \epsilon)$ | Bartlett et al. (2012) |
| osmotic potential at full turgor (pinot_node) (Eq. 6) | π_0 | MPa | Leaf: G [9.8,6.26], Stem, TRoot, ARoot: LN [0.32,0.39] | Bartlett et al. (2012, 2014, 2016) and Christoffersen et al. (2016) |
| bulk elastic modulus (epsil_node) (Eq. 7) | ϵ | MPa | Leaf: G (4.07, 4.12) Stem, TRoot and ARoot: G [3.57, 3.84] | Bartlett et al. (2012, 2014), and Christoffersen et al. (2016) |
| residual water fraction (resid_node) (Eq. 5) | RWC_r | unitless | Leaf: B [2.14,4.10] Stem, TRoot and ARoot: B [2.71, 4.53] | Bartlett et al. (2012, 2014), Christoffersen et al. (2016) |
| Vulnerability Curve (water potential – hydraulic conductivity relationship) | | | | |
| water potential at 50% loss of max conductivity (p50_node) (Eq. 3) | $P_{50,x}$ | MPa | Stem, TRoot and ARoot: G [2.07, 1.18] | Choat et al. (2012) |
| vulnerability curve shape parameter (avuln_node) (Eq. 3) | a_x | unitless | Stem, TRoot and ARoot: LN [0.82,0.66] | Choat et al. (2012) |
| xylem conductivity per unit sapwood area (kmax_node_stem) (Eq. 7) | $k_{s,max}$ | kg m ⁻¹ s ⁻¹ MPa ⁻¹ | G [1.41, 2.37] | Choat et al. (2012) |
| Leaf hydraulics | | | | |

| | | | | |
|---|-------------------|---|--|--|
| leaf water potential at 50% loss of max gs (p_{50_gs}) (Eq. 12) | $P_{50,gs}$ | MPa | G [5.73, 0.27] | Klein (2014) |
| stomatal vulnerability shape parameter (a_{vuln_gs}) (Eq. 12) | a_{gs} | unitless | $a_{gs} = -2.406 P_{50,gs} (-P_{50,gs})^{-1.25}$ | Christoffersen et al. (2016) |
| Leaf cuticular conductivity (k_{0_leaf}) (Eq. 11) | g_0 | $\mu\text{mol m}^{-2}\text{s}^{-1}$ | LN [1.04, 0.84] | This study (M. Slot, unpublished data) |
| Plant Hydraulic Architecture | | | | |
| Xylem taper exponent for sapwood (p_{taper}) (Eq. 9) | p | (-) | U (0.08, 0.5) | Savage et al. (2010) |
| Leaf area to sapwood area ratio (la_{2sa}) (Eq. 7) | $\frac{A_l}{A_s}$ | (-) | LN (-0.48, 0.77) | Choat et al. (2012) |
| Root hydraulic Traits | | | | |
| specific root length (srl) (Eq. 13) | srl | m g^{-1} | G [1.70, 35.31] | Iversen et al. (2017) |
| absorbing root radius (rs_2) (Eq. 13) | r | mm | LN [-1.91, 0.79] | Iversen et al. (2017) |
| fraction of total tree resistance that is aboveground (r_{frac_stem}) (Eq. 10) | $R_{frac,stem}$ | Unitless | U [0.1,0.7] | This study; empirical |
| root-soil interface conductivity per unit surface area (Kr_1) (Eq. 13) | $k_{r1,max}$ | $\text{kg m}^{-1} \text{s}^{-1}$ MPa^{-1} | G [1.41, 2.37] | This study; empirically set the same as xylem conductivity |
| maximum root water loss rate (Kr_2) (Eq. 14) | $k_{r2,max}$ | $\text{kg m}^{-1} \text{s}^{-1}$ MPa^{-1} | LN [-6.80, 0.92] | Wolfe (2020); Empirically set as 1/1000 bark water loss rate |

621 **Note:** 1:B-Beta distribution; U- Uniform distribution [lower limit, upper limit]; N-Gaussian distribution

622 (mean, standard deviation); LN-Log Normal Distribution [mean, standard deviation]; G-Gamma

623 distribution (lambda, scale); TRoot-Transporting root; ARoot-Absorbing root.

624

625 **Reference**

- 626 Adams, H. D., Zeppel, M. J. B., Anderegg, W. R. L., Hartmann, H., Landhausser, S. M., Tissue,
627 D. T., Huxman, T. E., Hudson, P. J., Franz, T. E., Allen, C. D., Anderegg, L. D. L., Barron-
628 Gafford, G. A., Beerling, D. J., Breshears, D. D., Brodrigg, T. J., Bugmann, H., Cobb, R. C.,
629 Collins, A. D., Dickman, L. T., Duan, H. L., Ewers, B. E., Galiano, L., Galvez, D. A., Garcia-
630 Forner, N., Gaylord, M. L., Germino, M. J., Gessler, A., Hacke, U. G., Hakamada, R., Hector,
631 A., Jenkins, M. W., Kane, J. M., Kolb, T. E., Law, D. J., Lewis, J. D., Limousin, J. M., Love, D.
632 M., Macalady, A. K., Martinez-Vilalta, J., Mencuccini, M., Mitchell, P. J., Muss, J. D., O'Brien,
633 M. J., O'Grady, A. P., Pangle, R. E., Pinkard, E. A., Piper, F. I., Plaut, J. A., Pockman, W. T.,
634 Quirk, J., Reinhardt, K., Ripullone, F., Ryan, M. G., Sala, A., Sevanto, S., Sperry, J. S., Vargas,
635 R., Vennetier, M., Way, D. A., Xu, C. G., Yezpez, E. A., and McDowell, N. G.: A multi-species
636 synthesis of physiological mechanisms in drought-induced tree mortality, *Nat Ecol Evol*, 1,
637 1285-1291, 10.1038/s41559-017-0248-x, 2017.
- 638 Anderegg, W. R. L., Klein, T., Bartlett, M., Sack, L., Pellegrini, A. F. A., Choat, B., and Jansen,
639 S.: Meta-analysis reveals that hydraulic traits explain cross-species patterns of drought-induced
640 tree mortality across the globe, *P Natl Acad Sci USA*, 113, 5024-5029,
641 10.1073/pnas.1525678113, 2016.
- 642 Anderegg, W. R. L., Konings, A. G., Trugman, A. T., Yu, K. L., Bowling, D. R., Gabbitas, R.,
643 Karp, D. S., Pacala, S., Sperry, J. S., Sulman, B. N., and Zenes, N.: Hydraulic diversity of forests
644 regulates ecosystem resilience during drought, *Nature*, 561, 538–541, 10.1038/s41586-018-0539-
645 7, 2018.
- 646 Arora, V. K., Katavouta, A., Williams, R. G., Jones, C. D., Brovkin, V., Friedlingstein, P.,
647 Schwinger, J., Bopp, L., Boucher, O., Cadule, P., Chamberlain, M. A., Christian, J. R., Delire,
648 C., Fisher, R. A., Hajima, T., Ilyina, T., Joetzjer, E., Kawamiya, M., Koven, C. D., Krasting, J.
649 P., Law, R. M., Lawrence, D. M., Lenton, A., Lindsay, K., Pongratz, J., Raddatz, T., Seferian,
650 R., Tachiiri, K., Tjiputra, J. F., Wiltshire, A., Wu, T. W., and Ziehn, T.: Carbon-concentration
651 and carbon-climate feedbacks in CMIP6 models and their comparison to CMIP5 models,
652 *Biogeosciences*, 17, 4173-4222, 10.5194/bg-17-4173-2020, 2020.
- 653 Bartlett, M. K., Scoffoni, C., and Sack, L.: The determinants of leaf turgor loss point and
654 prediction of drought tolerance of species and biomes: a global meta-analysis, *Ecol Lett*, 15, 393-
655 405, 10.1111/j.1461-0248.2012.01751.x, 2012.
- 656 Bartlett, M. K., Klein, T., Jansen, S., Choat, B., and Sack, L.: The correlations and sequence of
657 plant stomatal, hydraulic, and wilting responses to drought, *P Natl Acad Sci USA*, 113, 13098-
658 13103, 10.1073/pnas.1604088113, 2016.
- 659 Bartlett, M. K., Zhang, Y., Kreidler, N., Sun, S. W., Ardy, R., Cao, K. F., and Sack, L.: Global
660 analysis of plasticity in turgor loss point, a key drought tolerance trait, *Ecol Lett*, 17, 1580-1590,
661 10.1111/ele.12374, 2014.
- 662 Bennett, A. C., McDowell, N. G., Allen, C. D., and Anderson-Teixeira, K. J.: Larger trees suffer
663 most during drought in forests worldwide, *Nat Plants*, 1, Artn 15139
664 10.1038/Nplants.2015.139, 2015.
- 665 Berenguer, E., Lennox, G. D., Ferreira, J., Malhi, Y., Aragao, L. E. O. C., Barreto, J. R.,
666 Espirito-Santo, F. D., Figueiredo, A. E. S., Franca, F., Gardner, T. A., Joly, C. A., Palmeira, A.
667 F., Quesada, C. A., Rossi, L. C., de Seixas, M. M. M., Smith, C. C., Withey, K., and Barlow, J.:
668 Tracking the impacts of El Nino drought and fire in human-modified Amazonian forests, *P Natl
669 Acad Sci USA*, 118, ARTN e2019377118: 10.1073/pnas.2019377118, 2021.

670 Bhagat, N., Raghav, M., Dubey, S., and Bedi, N.: Bacterial Exopolysaccharides: Insight into
671 Their Role in Plant Abiotic Stress Tolerance, *J Microbiol Biotechnol*, 31, 1045-1059,
672 10.4014/jmb.2105.05009, 2021.

673 Binks, O., Meir, P., Rowland, L., da Costa, A. C. L., Vasconcelos, S. S., de Oliveira, A. A. R.,
674 Ferreira, L., Christoffersen, B., Nardini, A., and Mencuccini, M.: Plasticity in leaf-level water
675 relations of tropical rainforest trees in response to experimental drought, *New Phytol*, 211, 477-
676 488, 10.1111/nph.13927, 2016.

677 Bonal, D., Burban, B., Stahl, C., Wagner, F., and Herault, B.: The response of tropical rainforests
678 to drought-lessons from recent research and future prospects, *Ann Forest Sci*, 73, 27-44,
679 10.1007/s13595-015-0522-5, 2016.

680 Bonan, G. B.: Forests and climate change: Forcings, feedbacks, and the climate benefits of
681 forests, *Science*, 320, 1444-1449, 10.1126/science.1155121, 2008.

682 Boyle, B., Hopkins, N., Lu, Z., Raygoza Garay, J. A., Mozzherin, D., Rees, T., Matasci, N.,
683 Narro, M. L., Piel, W. H., and McKay, S. J.: The taxonomic name resolution service: an online
684 tool for automated standardization of plant names, *BMC bioinformatics*, 14, 1-15, 2013.

685 Breshears, D. D., Myers, O. B., Meyer, C. W., Barnes, F. J., Zou, C. B., Allen, C. D., McDowell,
686 N. G., and Pockman, W. T.: Tree die-off in response to global change-type drought: mortality
687 insights from a decade of plant water potential measurements, *Front Ecol Environ*, 7, 185-189,
688 10.1890/080016, 2009.

689 Caldwell, P. M., Mametjanov, A., Tang, Q., Van Roekel, L. P., Golaz, J. C., Lin, W. Y., Bader,
690 D. C., Keen, N. D., Feng, Y., Jacob, R., Maltrud, M. E., Roberts, A. F., Taylor, M. A.,
691 Veneziani, M., Wang, H. L., Wolfe, J. D., Balaguru, K., Cameron-Smith, P., Dong, L., Klein, S.
692 A., Leung, L. R., Li, H. Y., Li, Q., Liu, X. H., Neale, R. B., Pinheiro, M., Qian, Y., Ullrich, P.
693 A., Xie, S. C., Yang, Y., Zhang, Y. Y., Zhang, K., and Zhou, T.: The DOE E3SM Coupled
694 Model Version 1: Description and Results at High Resolution, *J Adv Model Earth Sy*, 11, 4095-
695 4146, 10.1029/2019ms001870, 2019.

696 Chen, J. W., Zhang, Q., Li, X. S., and Cao, K. F.: Independence of stem and leaf hydraulic traits
697 in six Euphorbiaceae tree species with contrasting leaf phenology, *Planta*, 230, 459-468,
698 10.1007/s00425-009-0959-6, 2009.

699 Chitra-Tarak, R., Xu, C. G., Aguilar, S., Anderson-Teixeira, K. J., Chambers, J., Detto, M.,
700 Faybishenko, B., Fisher, R. A., Knox, R. G., Koven, C. D., Kueppers, L. M., Kunert, N., Kupers,
701 S. J., McDowell, N. G., Newman, B. D., Paton, S. R., Perez, R., Ruiz, L., Sack, L., Warren, J.
702 M., Wolfe, B. T., Wright, C., Wright, S. J., Zailaa, J., and McMahon, S. M.: Hydraulically-
703 vulnerable trees survive on deep-water access during droughts in a tropical forest, *New Phytol*,
704 231, 1798-1813, 10.1111/nph.17464, 2021.

705 Choat, B., Jansen, S., Brodribb, T. J., Cochard, H., Delzon, S., Bhaskar, R., Bucci, S. J., Feild, T.
706 S., Gleason, S. M., Hacke, U. G., Jacobsen, A. L., Lens, F., Maherali, H., Martinez-Vilalta, J.,
707 Mayr, S., Mencuccini, M., Mitchell, P. J., Nardini, A., Pittermann, J., Pratt, R. B., Sperry, J. S.,
708 Westoby, M., Wright, I. J., and Zanne, A. E.: Global convergence in the vulnerability of forests
709 to drought, *Nature*, 491, 752-+, 10.1038/nature11688, 2012.

710 Christoffersen, B. O., Gloor, M., Fauset, S., Fyllas, N. M., Galbraith, D. R., Baker, T. R., Kruijt,
711 B., Rowland, L., Fisher, R. A., Binks, O. J., Sevanto, S., Xu, C. G., Jansen, S., Choat, B.,
712 Mencuccini, M., McDowell, N. G., and Meir, P.: Linking hydraulic traits to tropical forest
713 function in a size-structured and trait-driven model (TFS v.1-Hydro), *Geosci Model Dev*, 9,
714 4227-4255, 10.5194/gmd-9-4227-2016, 2016.

715 Dichio, B., Xiloyannis, C., Sofo, A., and Montanaro, G.: Osmotic regulation in leaves and roots
716 of olive trees during a water deficit and rewatering, *Tree Physiol*, 26, 179-185, DOI
717 10.1093/treephys/26.2.179, 2006.

718 Fang, Y. L., Leung, L. R., Knox, R., Koven, C., and Bond-Lamberty, B.: Impact of the numerical
719 solution approach of a plant hydrodynamic model (v0.1) on vegetation dynamics, *Geosci Model*
720 *Dev*, 15, 6385-6398, 10.5194/gmd-15-6385-2022, 2022.

721 Fisher, R., McDowell, N., Purves, D., Moorcroft, P., Sitch, S., Cox, P., Huntingford, C., Meir, P.,
722 and Woodward, F. I.: Assessing uncertainties in a second-generation dynamic vegetation model
723 caused by ecological scale limitations, *New Phytol*, 187, 666-681, 10.1111/j.1469-
724 8137.2010.03340.x, 2010.

725 Fisher, R. A. and Koven, C. D.: Perspectives on the Future of Land Surface Models and the
726 Challenges of Representing Complex Terrestrial Systems, *J Adv Model Earth Sy*, 12, ARTN
727 e2018MS001453: 10.1029/2018MS001453, 2020.

728 Fisher, R. A., Muszala, S., Versteinstein, M., Lawrence, P., Xu, C., McDowell, N. G., Knox, R.
729 G., Koven, C., Holm, J., Rogers, B. M., Spessa, A., Lawrence, D., and Bonan, G.: Taking off the
730 training wheels: the properties of a dynamic vegetation model without climate envelopes,
731 *CLM4.5(ED)*, *Geosci Model Dev*, 8, 3593-3619, 10.5194/gmd-8-3593-2015, 2015.

732 Fisher, R. A., Koven, C. D., Anderegg, W. R. L., Christoffersen, B. O., Dietze, M. C., Farrior, C.
733 E., Holm, J. A., Hurtt, G. C., Knox, R. G., Lawrence, P. J., Lichstein, J. W., Longo, M.,
734 Matheny, A. M., Medvigy, D., Muller-Landau, H. C., Powell, T. L., Serbin, S. P., Sato, H.,
735 Shuman, J. K., Smith, B., Trugman, A. T., Viskari, T., Verbeeck, H., Weng, E. S., Xu, C. G., Xu,
736 X. T., Zhang, T., and Moorcroft, P. R.: Vegetation demographics in Earth System Models: A
737 review of progress and priorities, *Global Change Biol*, 24, 35-54, 10.1111/gcb.13910, 2018.

738 Gleason, S. M., Westoby, M., Jansen, S., Choat, B., Hacke, U. G., Pratt, R. B., Bhaskar, R.,
739 Brodribb, T. J., Bucci, S. J., Cao, K. F., Cochard, H., Delzon, S., Domec, J. C., Fan, Z. X., Feild,
740 T. S., Jacobsen, A. L., Johnson, D. M., Lens, F., Maherali, H., Martinez-Vilalta, J., Mayr, S.,
741 McCulloh, K. A., Mencuccini, M., Mitchell, P. J., Morris, H., Nardini, A., Pittermann, J.,
742 Plavcova, L., Schreiber, S. G., Sperry, J. S., Wright, I. J., and Zanne, A. E.: Weak tradeoff
743 between xylem safety and xylem-specific hydraulic efficiency across the world's woody plant
744 species, *New Phytol*, 209, 123-136, 10.1111/nph.13646, 2016.

745 Hammond, W. M., Yu, K., Wilson, L. A., Will, R. E., Anderegg, W. R. L., and Adams, H. D.:
746 Dead or dying? Quantifying the point of no return from hydraulic failure in drought-induced tree
747 mortality, *New Phytol*, 223, 1834-1843, <https://doi.org/10.1111/nph.15922>, 2019.

748 Hochberg, U., Rockwell, F. E., Holbrook, N. M., and Cochard, H.: Iso/Anisohydry: A Plant-
749 Environment Interaction Rather Than a Simple Hydraulic Trait, *Trends Plant Sci*, 23, 112-120,
750 10.1016/j.tplants.2017.11.002, 2018.

751 Huang, M. Y., Xu, Y., Longo, M., Keller, M., Knox, R. G., Koven, C. D., and Fisher, R. A.:
752 Assessing impacts of selective logging on water, energy, and carbon budgets and ecosystem
753 dynamics in Amazon forests using the Functionally Assembled Terrestrial Ecosystem Simulator,
754 *Biogeosciences*, 17, 4999-5023, 10.5194/bg-17-4999-2020, 2020.

755 Iversen, C. M., McCormack, M. L., Powell, A. S., Blackwood, C. B., Freschet, G. T., Kattge, J.,
756 Roumet, C., Stover, D. B., Soudzilovskaia, N. A., Valverde-Barrantes, O. J., van Bodegom, P.
757 M., and Violle, C.: A global Fine-Root Ecology Database to address below-ground challenges in
758 plant ecology, *New Phytol*, 215, 15-26, 10.1111/nph.14486, 2017.

759 Kennedy, D., Swenson, S., Oleson, K. W., Lawrence, D. M., Fisher, R., da Costa, A. C. L., and
 760 Gentine, P.: Implementing Plant Hydraulics in the Community Land Model, Version 5, *J Adv*
 761 *Model Earth Sy*, 11, 485-513, 10.1029/2018ms001500, 2019.
 762 Klein, T.: The variability of stomatal sensitivity to leaf water potential across tree species
 763 indicates a continuum between isohydric and anisohydric behaviours, *Funct Ecol*, 28, 1313-
 764 1320, 10.1111/1365-2435.12289, 2014.
 765 Koven, C. D., Knox, R. G., Fisher, R. A., Chambers, J. Q., Christoffersen, B. O., Davies, S. J.,
 766 Detto, M., Dietze, M. C., Faybishenko, B., Holm, J., Huang, M. Y., Kovenock, M., Kueppers, L.
 767 M., Lemieux, G., Massoud, E., McDowel, N. G., Muller-Landau, H. C., Needham, J. F., Norby,
 768 R. J., Powell, T., Rogers, A., Serbin, S. P., Shuman, J. K., Swann, A. L. S., Varadharajan, C.,
 769 Walker, A. P., Wright, S. J., and Xu, C. G.: Benchmarking and parameter sensitivity of
 770 physiological and vegetation dynamics using the Functionally Assembled Terrestrial Ecosystem
 771 Simulator (FATES) at Barro Colorado Island, Panama, *Biogeosciences*, 17, 3017-3044,
 772 10.5194/bg-17-3017-2020, 2020.
 773 Kunert, N., Zailaa, J., Herrmann, V., Muller-Landau, H. C., Wright, S. J., Perez, R., McMahon,
 774 S. M., Condit, R. C., Hubbell, S. P., Sack, L., Davies, S. J., and Anderson-Teixeira, K. J.: Leaf
 775 turgor loss point shapes local and regional distributions of evergreen but not deciduous tropical
 776 trees, *New Phytol*, 230, 485-496, 10.1111/nph.17187, 2021.
 777 Kursar, T. A., Engelbrecht, B. M. J., Burke, A., Tyree, M. T., El Omari, B., and Giraldo, J. P.:
 778 Tolerance to low leaf water status of tropical tree seedlings is related to drought performance and
 779 distribution, *Funct Ecol*, 23, 93-102, 10.1111/j.1365-2435.2008.01483.x, 2009.
 780 Lambert, M. S. A., Tang, H., Aas, K. S., Stordal, F., Fisher, R. A., Fang, Y. L., Ding, J. Y., and
 781 Parmentier, F. J. W.: Inclusion of a cold hardening scheme to represent frost tolerance is
 782 essential to model realistic plant hydraulics in the Arctic-boreal zone in CLM5.0-FATES-Hydro,
 783 *Geosci Model Dev*, 15, 8809-8829, 10.5194/gmd-15-8809-2022, 2022.
 784 Lawrence, D. M., Fisher, R. A., Koven, C. D., Oleson, K. W., Swenson, S. C., Bonan, G.,
 785 Collier, N., Ghimire, B., van Kampenhout, L., Kennedy, D., Kluzek, E., Lawrence, P. J., Li, F.,
 786 Li, H. Y., Lombardozzi, D., Riley, W. J., Sacks, W. J., Shi, M. J., Vertenstein, M., Wieder, W.
 787 R., Xu, C. G., Ali, A. A., Badger, A. M., Bisht, G., van den Broeke, M., Brunke, M. A., Burns, S.
 788 P., Buzan, J., Clark, M., Craig, A., Dahlin, K., Drewniak, B., Fisher, J. B., Flanner, M., Fox, A.
 789 M., Gentine, P., Hoffman, F., Keppel-Aleks, G., Knox, R., Kumar, S., Lenaerts, J., Leung, L. R.,
 790 Lipscomb, W. H., Lu, Y. Q., Pandey, A., Pelletier, J. D., Perket, J., Randerson, J. T., Ricciuto, D.
 791 M., Sanderson, B. M., Slater, A., Subin, Z. M., Tang, J. Y., Thomas, R. Q., Martin, M. V., and
 792 Zeng, X. B.: The Community Land Model Version 5: Description of New Features,
 793 Benchmarking, and Impact of Forcing Uncertainty, *J Adv Model Earth Sy*, 11, 4245-4287,
 794 10.1029/2018ms001583, 2019.
 795 Manzoni, S., Vico, G., Katul, G., Palmroth, S., Jackson, R. B., and Porporato, A.: Hydraulic
 796 limits on maximum plant transpiration and the emergence of the safety-efficiency trade-off, *New*
 797 *Phytol*, 198, 169-178, 10.1111/nph.12126, 2013.
 798 Massoud, E. C., Xu, C. G., Fisher, R. A., Knox, R. G., Walker, A. P., Serbin, S. P.,
 799 Christoffersen, B. O., Holm, J. A., Kueppers, L. M., Ricciuto, D. M., Wei, L., Johnson, D. J.,
 800 Chambers, J. Q., Koven, C. D., McDowell, N. G., and Vrugt, J. A.: Identification of key
 801 parameters controlling demographically structured vegetation dynamics in a land surface model:
 802 CLM4.5(FATES), *Geosci Model Dev*, 12, 4133-4164, 10.5194/gmd-12-4133-2019, 2019.
 803 McDowell, N., Allen, C. D., Anderson-Teixeira, K., Brando, P., Brienen, R., Chambers, J.,
 804 Christoffersen, B., Davies, S., Doughty, C., Duque, A., Espirito-Santo, F., Fisher, R., Fontes, C.

805 G., Galbraith, D., Goodsman, D., Grossiord, C., Hartmann, H., Holm, J., Johnson, D. J., Kassim,
806 A., Keller, M., Koven, C., Kueppers, L., Kumagai, T., Malhi, Y., McMahon, S. M., Mencuccini,
807 M., Meir, P., Moorcroft, P., Muller-Landau, H. C., Phillips, O. L., Powell, T., Sierra, C. A.,
808 Sperry, J., Warren, J., Xu, C. G., and Xu, X. T.: Drivers and mechanisms of tree mortality in
809 moist tropical forests, *New Phytol*, 219, 851-869, 10.1111/nph.15027, 2018.

810 McDowell, N. G., Fisher, R. A., Xu, C. G., Domec, J. C., Holtta, T., Mackay, D. S., Sperry, J. S.,
811 Boutz, A., Dickman, L., Gehres, N., Limousin, J. M., Macalady, A., Martinez-Vilalta, J.,
812 Mencuccini, M., Plaut, J. A., Ogee, J., Pangle, R. E., Rasse, D. P., Ryan, M. G., Sevanto, S.,
813 Waring, R. H., Williams, A. P., Yezpez, E. A., and Pockman, W. T.: Evaluating theories of
814 drought-induced vegetation mortality using a multimodel-experiment framework, *New Phytol*,
815 200, 304-321, 10.1111/nph.12465, 2013.

816 McDowell, N. G., Sapes, G., Pivovarov, A., Adams, H. D., Allen, C. D., Anderegg, W. R. L.,
817 Arend, M., Breshears, D. D., Brodrigg, T., Choat, B., Cochard, H., De Caceres, M., De Kauwe,
818 M. G., Grossiord, C., Hammond, W. M., Hartmann, H., Hoch, G., Kahmen, A., Klein, T.,
819 Mackay, D. S., Mantova, M., Martinez-Vilalta, J., Medlyn, B. E., Mencuccini, M., Nardini, A.,
820 Oliveira, R. S., Sala, A., Tissue, D. T., Torres-Ruiz, J. M., Trowbridge, A. M., Trugman, A. T.,
821 Wiley, E., and Xu, C. G.: Mechanisms of woody-plant mortality under rising drought, CO₂ and
822 vapour pressure deficit, *Nat Rev Earth Env*, 3, 294-308, 10.1038/s43017-022-00272-1, 2022.

823 Moorcroft, P. R., Hurtt, G. C., and Pacala, S. W.: A method for scaling vegetation dynamics: The
824 ecosystem demography model (ED), *Ecol Monogr*, 71, 557-585, 10.1890/0012-
825 9615(2001)071[0557:Amsfvd]2.0.Co;2, 2001.

826 Needham, J. F., Chambers, J., Fisher, R., Knox, R., and Koven, C. D.: Forest responses to
827 simulated elevated CO₂ under alternate hypotheses of size- and age-dependent mortality, *Global*
828 *Change Biol*, 26, 5734-5753, 10.1111/gcb.15254, 2020.

829 Norman, J.: Modelling the complete crop canopy, in *Modification of the Aerial Environment of*
830 *Plants*, *Am. Soc. Agri. Eng. Monograph*, 2, 249-277, 1979.

831 North, G. B. and Nobel, P. S.: Drought-Induced Changes in Hydraulic Conductivity and
832 Structure in Roots of *Ferocactus-Acanthodes* and *Opuntia-Ficus-Indica*, *New Phytol*, 120, 9-19,
833 DOI 10.1111/j.1469-8137.1992.tb01053.x, 1992.

834 Oleson, K. W., Lawrence, D. M., Bonan, G. B., Drewniak, B., Huang, M., Koven, C. D., Levis,
835 S., Li, F., Riley, W. J., Subin, Z. M., Swenson, S. C., Thornton, P. E., Bozbiyik, A., Fisher, R.,
836 Heald, C. L., Kluzek, E., Lamarque, J.-F., Lawrence, P. J., Leung, L. R., Lipscomb, W.,
837 Muszala, S., Ricciuto, D. M., Sacks, W., Sun, Y., Tang, J., & Yang, Z.-L. : Technical description
838 of version 4.5 of the Community Land Model (CLM) National Center for Atmospheric Research,
839 Boulder, Colorado, USA. Tech. Rep. NCAR/TN-503+STR, 2013.

840 Olson, M. E., Anfodillo, T., Gleason, S. M., and McCulloh, K. A.: Tip-to-base xylem conduit
841 widening as an adaptation: causes, consequences, and empirical priorities, *New Phytol*, 229,
842 1877-1893, 10.1111/nph.16961, 2021.

843 Paton, S.: *Yearly Reports_Barro Colorado Island*, Smithsonian Tropical Research Institute,
844 <https://doi.org/10.25573/data.11799111.v3>, 2020.

845 Pineda-Garcia, F., Paz, H., and Meinzer, F. C.: Drought resistance in early and late secondary
846 successional species from a tropical dry forest: the interplay between xylem resistance to
847 embolism, sapwood water storage and leaf shedding, *Plant Cell Environ*, 36, 405-418,
848 10.1111/j.1365-3040.2012.02582.x, 2013.

849 Poudel, M., Mendes, R., Costa, L. A., Bueno, C. G., Meng, Y., Folimonova, S. Y., Garrett, K.
850 A., and Martins, S. J.: The role of plant-associated bacteria, fungi, and viruses in drought stress
851 mitigation, *Frontiers in microbiology*, 12, 3058, 2021.

852 Powell, T. L., Wheeler, J. K., de Oliveira, A. A. R., da Costa, A. C. L., Saleska, S. R., Meir, P.,
853 and Moorcroft, P. R.: Differences in xylem and leaf hydraulic traits explain differences in
854 drought tolerance among mature Amazon rainforest trees, *Global Change Biol*, 23, 4280-4293,
855 10.1111/gcb.13731, 2017.

856 Powell, T. L., Koven, C. D., Johnson, D. J., Faybishenko, B., Fisher, R. A., Knox, R. G.,
857 McDowell, N. G., Condit, R., Hubbell, S. P., Wright, S. J., Chambers, J. Q., and Kueppers, L.
858 M.: Variation in hydroclimate sustains tropical forest biomass and promotes functional diversity,
859 *New Phytol*, 219, 932-946, 10.1111/nph.15271, 2018.

860 Roderick, M. L., Berry, S. L., Saunders, A. R., and Noble, I. R.: On the relationship between the
861 composition, morphology and function of leaves, *Funct Ecol*, 13, 696-710, DOI 10.1046/j.1365-
862 2435.1999.00369.x, 1999.

863 Rodriguez-Zaccaro, F. D., Valdovinos-Ayala, J., Percolla, M. I., Venturas, M. D., Pratt, R. B.,
864 and Jacobsen, A. L.: Wood structure and function change with maturity: Age of the vascular
865 cambium is associated with xylem changes in current-year growth, *Plant, Cell & Environment*,
866 42, 1816-1831, <https://doi.org/10.1111/pce.13528>, 2019.

867 Rowland, L., da Costa, A. C. L., Galbraith, D. R., Oliveira, R. S., Binks, O. J., Oliveira, A. A. R.,
868 Pullen, A. M., Doughty, C. E., Metcalfe, D. B., Vasconcelos, S. S., Ferreira, L. V., Malhi, Y.,
869 Grace, J., Mencuccini, M., and Meir, P.: Death from drought in tropical forests is triggered by
870 hydraulics not carbon starvation, *Nature*, 528, 119+, 10.1038/nature15539, 2015.

871 Sack, L., Cowan, P. D., Jaikumar, N., and Holbrook, N. M.: The 'hydrology' of leaves: co-
872 ordination of structure and function in temperate woody species, *Plant Cell Environ*, 26, 1343-
873 1356, DOI 10.1046/j.0016-8025.2003.01058.x, 2003.

874 Savage, V. M., Bentley, L. P., Enquist, B. J., Sperry, J. S., Smith, D. D., Reich, P. B., and von
875 Allmen, E. I.: Hydraulic trade-offs and space filling enable better predictions of vascular
876 structure and function in plants, *P Natl Acad Sci USA*, 107, 22722-22727,
877 10.1073/pnas.1012194108, 2010.

878 Schmidhalter, U.: The gradient between pre-dawn rhizoplane and bulk soil matric potentials, and
879 its relation to the pre-dawn root and leaf water potentials of four species, *Plant, Cell &
880 Environment*, 20, 953-960, <https://doi.org/10.1046/j.1365-3040.1997.d01-136.x>, 1997.

881 Seneviratne, S. I., Zhang, X., Adnan, M., Badi, W., Dereczynski, C., Luca, A. D., Ghosh, S.,
882 Iskandar, I., Kossin, J., Lewis, S., Otto, F., Pinto, I., Satoh, M., Vicente-Serrano, S. M., Wehner,
883 M., Zhou, B., and Allan, R.: Weather and climate extreme events in a changing climate, in:
884 *Climate Change 2021: The Physical Science Basis: Working Group I contribution to the Sixth
885 Assessment Report of the Intergovernmental Panel on Climate Change*, edited by: Masson-
886 Delmotte, V. P., Zhai, A., Pirani, S. L., and Connors, C., Cambridge University Press,
887 Cambridge, UK, 1513-1766, 2021.

888 Shinozaki, K., Yoda, K., Hozumi, K., and Kira, T.: A quantitative analysis of plant form-the pipe
889 model theory: I. Basic analyses, *Japanese Journal of ecology*, 14, 97-105, 1964.

890 Smith, D. D., Sperry, J. S., Enquist, B. J., Savage, V. M., McCulloh, K. A., and Bentley, L. P.:
891 Deviation from symmetrically self-similar branching in trees predicts altered hydraulics,
892 mechanics, light interception and metabolic scaling, *New Phytol*, 201, 217-229,
893 10.1111/nph.12487, 2014.

894 Sperry, J. S. and Love, D. M.: What plant hydraulics can tell us about responses to climate-
895 change droughts, *New Phytol*, 207, 14-27, 10.1111/nph.13354, 2015.

896 Su, R., Liu, H., Wang, C., Zhang, H., and Cui, J.: Leaf turgor loss point is one of the best
897 predictors of drought-induced tree mortality in tropical forest, *Front Ecol Evol*, 10, ARTN
898 974004: 10.3389/fevo.2022.974004, 2022.

899 Tyree, M. T. and Yang, S.: Water-storage capacity of Thuja, Tsuga and Acer stems measured by
900 dehydration isotherms: the contribution of capillary water and cavitation, *Planta*, 182, 420-426,
901 1990.

902 Wei, L., Xu, C. G., Jansen, S., Zhou, H., Christoffersen, B. O., Pockman, W. T., Middleton, R.
903 S., Marshall, J. D., and McDowell, N. G.: A heuristic classification of woody plants based on
904 contrasting shade and drought strategies, *Tree Physiol*, 39, 767-781, 10.1093/treephys/tpy146,
905 2019.

906 Wolfe, B. T.: Bark water vapour conductance is associated with drought performance in tropical
907 trees, *Biol Letters*, 16, ARTN 20200263: 10.1098/rsbl.2020.0263, 2020.

908 Wright, S. J., Kitajima, K., Kraft, N. J. B., Reich, P. B., Wright, I. J., Bunker, D. E., Condit, R.,
909 Dalling, J. W., Davies, S. J., Diaz, S., Engelbrecht, B. M. J., Harms, K. E., Hubbell, S. P., Marks,
910 C. O., Ruiz-Jaen, M. C., Salvador, C. M., and Zanne, A. E.: Functional traits and the growth-
911 mortality trade-off in tropical trees, *Ecology*, 91, 3664-3674, Doi 10.1890/09-2335.1, 2010.

912 Xu, C. G. and Gertner, G.: Understanding and comparisons of different sampling approaches for
913 the Fourier Amplitudes Sensitivity Test (FAST), *Comput Stat Data An*, 55, 184-198,
914 10.1016/j.csda.2010.06.028, 2011a.

915 Xu, C. G. and Gertner, G. Z.: Reliability of global sensitivity indices, *J Stat Comput Sim*, 81,
916 1939-1969, 10.1080/00949655.2010.509317, 2011b.

917 Xu, C. G., McDowell, N. G., Fisher, R. A., Wei, L., Sevanto, S., Christoffersen, B. O., Weng, E.
918 S., and Middleton, R. S.: Increasing impacts of extreme droughts on vegetation productivity
919 under climate change, *Nat Clim Change*, 9, 948+, 10.1038/s41558-019-0630-6, 2019.

920 Xu, X. T., Medvigy, D., Powers, J. S., Becknell, J. M., and Guan, K. Y.: Diversity in plant
921 hydraulic traits explains seasonal and inter-annual variations of vegetation dynamics in
922 seasonally dry tropical forests, *New Phytol*, 212, 80-95, 10.1111/nph.14009, 2016.

923 Yang, S. D. and Tyree, M. T.: Hydraulic Resistance in Acer-Saccharum Shoots and Its Influence
924 on Leaf Water Potential and Transpiration, *Tree Physiol*, 12, 231-242, DOI
925 10.1093/treephys/12.3.231, 1993.

926